④

AD-A197 310

AD

TECHNICAL REPORT ARCCB-TR-88016

FRACTURE AND FATIGUE

R. O. RITCHIE

W. W. GERBERICH

J. H. UNDERWOOD

DTIC
ELECTE
JUL 1 1 1988
S
H
D

APRIL 1988

DISCLAIMER

The findings in this report are not to be construed as an official Department of the Army position unless so designated by other authorized documents.

The use of trade name(s) and/or manufacturer(s) does not constitute an official indorsement or approval.

DESTRUCTION NOTICE

For classified documents, follow the procedures in DoD 5200.22-M, Industrial Security Manual, Section II-19 or DoD 5200.1-R, Information Security Program Regulation, Chapter IX.

For unclassified, limited documents, destroy by any method that will prevent disclosure of contents or reconstruction of the document.

For unclassified, unlimited documents, destroy when the report is no longer needed. Do not return it to the originator.

REPORT DOCUMENTATION PAGE		READ INSTRUCTIONS BEFORE COMPLETING FORM
1. REPORT NUMBER ARCCB-TR-88016	2. GOVT ACCESSION NO.	3. RECIPIENT'S CATALOG NUMBER
4. TITLE (and Subtitle) FRACTURE AND FATIGUE		5. TYPE OF REPORT & PERIOD COVERED Final
		6. PERFORMING ORG. REPORT NUMBER
7. AUTHOR(s) R. O. Ritchie, W. W. Gerberich, and J. H. Underwood (See Reverse)		8. CONTRACT OR GRANT NUMBER(s)
9. PERFORMING ORGANIZATION NAME AND ADDRESS US Army Armament Research, Develop, & Engr Center Benet Laboratories, SMCAR-CCB-TL Watervliet, NY 12189-4050		10. PROGRAM ELEMENT, PROJECT, TASK AREA & WORK UNIT NUMBERS AMCMS No. 694000084 PRON No. AW6MC00103AW1A
11. CONTROLLING OFFICE NAME AND ADDRESS US Army Armament Research, Develop, & Engr Center Close Combat Armaments Center Picatinny Arsenal, NJ 07806-5000		12. REPORT DATE April 1988
		13. NUMBER OF PAGES 69
14. MONITORING AGENCY NAME & ADDRESS(if different from Controlling Office)		15. SECURITY CLASS. (of this report) UNCLASSIFIED
		15a. DECLASSIFICATION/DOWNGRADING SCHEDULE

16. DISTRIBUTION STATEMENT (of this Report)

Approved for public release; distribution unlimited.

17. DISTRIBUTION STATEMENT (of the abstract entered in Block 20, if different from Report)

19. KEY WORDS (Continue on reverse side if necessary and identify by block number)

Fracture Mechanics
Fatigue
Concepts
Micromechanisms
Environmental Effects

20. ABSTRACT (Continue on reverse side if necessary and identify by block number)

This report has attempted to provide, with necessary brevity, a basic frame-
work for understanding the macroscopic and microscopic aspects of fracture and
fatigue crack propagation in engineering materials from a fracture mechanics
viewpoint. Further details may be obtained with reference to the attached
bibliography.

(CONT'D ON REVERSE)

DD FORM 1473 EDITION OF 1 NOV 65 IS OBSOLETE

7. AUTHORS (CONT'D)

R. O. Ritchie
Department of Materials Science and Mineral Engineering
University of California
Berkeley, CA 94720

W. W. Gerberich
Department of Chemical Engineering and Materials Science
University of Minnesota
Minneapolis, MN 55445

20. ABSTRACT (CONT'D)

In the last twenty years, much progress has been made with the continuum
mechanics characterization of crack growth rates through the application of
linear elastic and elastic-plastic fracture mechanics, and such analyses are
now in widespread use for defect-tolerant design codes. Similarly, an
understanding of the role of microstructure in improving the resistance to
fracture and fatigue has emerged to the point where alloy design guidelines
exist for the production of alloys with optimum resistance to fatigue failure.
However, much work remains in the definition of mechanisms associated with
environmentally-influenced crack growth, with the effect of variable amplitude
loading, with the problem of the short flaw, and in the fracture of
microscopic structures (e.g., packaging problems in the electronics industry).
These problems demand an interdisciplinary approach to fracture and fatigue
research involving applied mechanics, materials science, and surface chemistry
studies, and clearly offer substantial opportunities for further
investigations both of fundamental nature and to provide reliable engineering
data needed in the design and maintenance of fracture and fatigue-critical
structures.

(keywords)

DTIC
COPY
INSPECTED
6

Accession For	
NTIS GRA&I	☑
DTIC TAB	☐
Unannounced	☐
Justification	

| By |
| Distribution/ |
| Availability Codes |

Dist	Avail and/or Special
A-1	

TABLE OF CONTENTS

i

TABLES

LIST OF ILLUSTRATIONS

GLOSSARY

Cleavage fracture   Brittle fracture mode which results from a transgranular low energy separation of crystallographic planes.

Crack closure   Contact between the surface of a fatigue crack during the unloading cycle, which leads to a reduction in the local "crack driving force."

Extrinsic toughening   Processes which impede the propagation of cracks by lowering the local "crack driving force", e.g., by crack tip shielding.

Fatigue   Failure of a material through repeated action of cyclic stresses.

Fracture toughness   A measure of a material's resistance to fracture as defined by a critical value of the stress intensity (K_{Ic}) or J-integral (J_{Ic}).

Intrinsic toughening   Processes which impede the propagation of cracks by increasing the microstructural resistance.

Intergranular cracking   A brittle mode of fracture resulting from separation along grain boundary surfaces.

J-integral   Scalar amplitude factor which uniquely characterizes the nonlinear elastic crack tip stress and deformation fields.

Microvoid coalescence	A ductile mode of fracture resulting from the nucleation, growth, and eventual coalescence of voids, generally formed at particles within the material.
Plastic zone size	A region of plastic deformation in the immediate vicinity of the crack tip.
Stress intensity factor	Scalar amplitude factor which uniquely characterizes the linear elastic crack tip stress and deformation fields.

The failure of structures and components in service by the processes of fracture and fatigue, i.e., monotonic or cyclically varying loads, respectively, represents one of the most damaging technological factors limiting the efficiency of industry today. It is seen for example in the failure of a tiny soldered joint in a printed circuit board in some strategic computer, the rupture of a large pressure vessel used to store lethal chemicals, or the loss of a commercial aircraft due to fracture of a structural section by fatigue. The topic is of such vital importance that the total cost of fracture in the U.S. alone, as assessed by a 1983 National Bureau of Standards report, is some $120 billion per year (approximately 4% of the GNP). In this article, the fundamental concepts underlying the mechanics and mechanisms of fracture and fatigue cracking are presented from both continuum and microstructural viewpoints. This includes a description of fracture mechanics, which is used to quantify failure under monotonic and cyclic loading, and of the microstructural origins of failure in engineering materials.

I. CONTINUUM APPROACH TO FRACTURE

A. Concepts of Fracture Mechanics

The concepts of fracture mechanics are basic ideas for developing methods of predicting the load-carrying capabilities of structures and components containing cracks. The concepts deal

1

with basic quantities or parameters of fracture mechanics. These quantities can be discussed in relation to the example of a center crack in a plate remotely loaded by a uniform tensile stress (See Fig. 1). When the half-crack length, a, is less than 10% of the total plate width, the relationship among stress-intensity factor, K, applied stress, σ, and half-crack length, a, is very close to the relationship for a crack in an infinitely wide plate, which is:

$$K = \sigma\sqrt{\pi a} \qquad (1)$$

The stress applied to the component, the length of the crack, and the stress-intensity factor in the loaded component with a crack are the basic quantities of fracture mechanics. The example in Fig. 1 also provides a simple explanation for the units of stress-intensity factor, i.e., the product of stress and square root of length. But more important is the concept that the stress-intensity factor, K, is a single parameter which includes both the effect of the stress applied to a sample and the effect of a crack of a given size in a sample. Still using the example of Fig. 1, if the combination of σ and a in Eq. 1 were to exceed a critical value of K, then the fracture strength of the plate would be exceeded and the crack would be expected to propagate. Mechanisms of such crack extension are described in Section II.

B. Energy Concepts

The origins of modern-day fracture mechanics may be traced to Griffith, who established an energy-release-rate criterion for brittle materials. Observations of the fracture strength of glass rods had shown that the longer the rod, the lower the strength. Thus the idea of a distribution of flaw sizes evolved, and it was discovered that the longer the rod, the larger the chance of finding a large natural flaw. This physical insight led to an instability criterion which involved the elastic energy released in a solid at the time a flaw grew catastrophically under an applied stress.

From the theory of elasticity comes the concept that the strain energy contained in an elastic body per unit volume is simply the area under the stress-strain curve, or:

$$U_0 = \sigma^2/2E \qquad (2)$$

where σ is the applied stress and E is Young's modulus. However, there is a reduction (that is, a release) of energy in an elastic body containing a flaw or a crack because of the inability of the unloaded crack surfaces to support a load. The volume of material whose energy is released is assumed to be the area of an elliptical region around the crack times the plate thickness, B; the volume is $\pi(2a)(a)B$. Then, the total energy released from the body due to the crack is the energy per unit volume times the volume, which is:

3

$$U = \pi(2a)(a)B \frac{\sigma^2}{2E} = \frac{\pi\sigma^2 a^2 B}{E} \qquad (3)$$

In ideally brittle solids, the released energy can be offset only by the surface energy absorbed, which is:

$$W = (2aB)(2\gamma_s) = 4aB\gamma_s \qquad (4)$$

where 2aB is the area of the crack and $2\gamma_s$ is twice the surface energy per unit area.

In essence, the Griffith's energy-balance criterion is that crack growth will occur when the amount of energy released due to an increment of crack advance is larger than the amount of energy absorbed:

$$dU/da \geq dW/da \qquad (5)$$

Performing the derivatives indicated in Eq. 5 and rearranging gives the Griffith criterion for crack growth:

$$\sigma\sqrt{\pi a} = \sqrt{2E\gamma_s} \qquad (6)$$

Fracture theory was built upon this criterion in the early 1940's by considering that the critical strain energy release rate, G_c, required for crack growth was equal to twice an effective surface energy, γ_{eff}:

4

$$G_c = 2\gamma_{eff} \tag{7}$$

This γ_{eff} is predominantly the plastic energy absorption around the crack tip, with only a small part due to the surface energy of the crack surfaces. Then, with the development of complex variable and numerical techniques to define the stress fields near cracks, this energy view was supplemented by stress concepts -- that is, the stress-intensity factor, K, and a critical value of K for crack growth, K_c. Replacing γ_s with γ_{eff} in Eq. 6 and noting that the energy and stress concepts are essentially identical (that is, K = $\sqrt{EG}$) gives:

$$K_c = \sqrt{EG_c} = \sigma\sqrt{\pi a} \tag{8}$$

which is the crack-growth-criterion equivalent of Eq. 1. Thus, K_c is the critical value of K which, when it is exceeded by a combination of applied stress and crack length, will lead to crack growth. For thick-plate plane-strain conditions, this critical value became known as the plane-strain fracture toughness, K_{Ic}, and any combination of applied stress and crack length that exceeds this value could produce unstable crack growth, as indicated schematically in Fig. 2(a) (Linear-elastic).

In work with tougher, lower-strength materials, it was later noted that stable slow crack growth could occur even though accompanied by considerable plastic deformation. Such phenomena

5

led to the nonlinear J-integral and R-curve concepts which could be used to predict the onset of stable slow crack growth and final instability under elastic-plastic conditions, as noted in Fig. 2(b). Finally, the fracture mechanics approach was applied to characterize subcritical crack growth phenomena where time-dependent slow crack growth, da/dt, or cyclic crack growth, da/dN, may be induced by special environments or fatigue loading. For combinations of stress and crack length above some environmental threshold, K_{Iscc}, or fatigue threshold ΔK_{TH}, subcritical growth occurs, as indicated in Fig. 2(c).

C. Detection of Flaws

To apply the above concepts, it is assumed that cracks or flaws exist in the body, and that these flaws can be detected prior to catastrophic failure. A great many failure investigations have confirmed the first assumption, that cracks exist in structural materials. In engineering design, materials are often considered to be free of cracklike flaws, but in reality flaws of some sort are always present in structural materials. The flaws may be so small or so unlike cracks that they will not become the sources of crack growth. However, the usefulness of the fracture mechanics approach is that it can predict what would happen if a cracklike flaw were to exist and to cause crack growth at a critical location of a component. Then, appropriate steps can be taken in design, manufacture and inspection to make sure that the flaw would be

6

detected before·the component is placed in service or that the undetected flaw would have no significant effect on the performance or lifetime of the component.

Nondestructive inspection methods are often used to detect flaws -- particularly in critical, highly stressed locations of structural components. Techniques include visual inspection, magnetic particle flux methods, ultrasonics and proof testing at stresses above those likely to be encountered in service. In general, however, the nondestructive testing method that is used should have the capability of detecting any flaw which could lead to failure during the lifetime of the component. The flawed component can then be withheld from service until its flaws are repaired. Regardless of the types and sizes of flaws which can be present in structural components, the important point is that nondestructive inspection methods can provide an indication of the flaw sizes. Then the maximum flaw size can be used to calculate the value of K, using an expression such as Eq. 1, and a quantitative description of the conditions for crack growth and failure can be made.

D. Characterizing Parameters

A second assumption implicit in the use of fracture mechanics is that a characteristic stress and deformation field surrounds any crack in a loaded body. The magnitude of this field, i.e., the stress intensity K for a linear elastic body, at the onset of crack

7

extension is a material property which is independent of specimen size and geometry for many conditions of loading and environment.

This approach makes possible a mathematical description of the stresses in the vicinity of the crack tip. This assumption of a crack in a linear-elastic solid at first appears contradictory to what is known about fracture of metals, because some plastic deformation is always found to accompany fracture. However, when the region of plastic deformation around the crack is small compared with the size of the crack, which often is true with large structures and with high-strength materials, this is a good assumption.

The description of the local crack tip field is achieved principally through asymptotic continuum mechanics analyses where the functional form of the local singular field is determined within a scalar amplitude factor whose magnitude is calculated from a complete analysis of the applied loading and geometry. For the linear-elastic behavior of a nominally stationary crack subjected to tensile (Mode I) opening, the local crack tip stresses (σ_{ij}) can be characterized in terms of the K_I singular field:

$$\sigma_{ij}(r,\theta) = \frac{K_I}{\sqrt{2\pi r}} f_{ij}(\theta) + 0(r^{\frac{1}{2}}) + \ldots$$

$$\rightarrow \frac{K_I}{\sqrt{2\pi r}} f_{ij}(\theta) \qquad \text{as } r \rightarrow 0 \qquad (9)$$

where K_I is the Mode I stress intensity factor, r the distance

8

ahead of the tip, θ the polar angle measured from the crack plane, and f_{ij} a dimensionless function of θ (Fig. 3). Provided this asymptotic field can be considered to "dominate" the local crack tip vicinity over a region which is large compared to the scale of microstructural deformation and fracture events involved, the scalar amplitude factor K_I can be considered as a single, configuration-independent parameter which uniquely and autonomously characterizes the local stress field ahead of a linear elastic crack and can be used as a correlator of crack extension.

The important implications of Eq. 9 are: (a) a crack in a loaded component or specimen generates its own intensified stress field near the crack tip, a stress field that differs from another crack-tip stress field only by the scaling factor represented by K; and (b) the factor K expresses how much the stress intensifies at the crack tip, and thereby allows the loading and geometry factors that influence crack growth in a specimen to be described on a uniform basis using a single parameter.

The stress-intensity factor, K, can have a simple relation to applied stress and crack length, as in Eq. 1. But, more often, the K relation is of greater complexity because of complex loading, various configurations of real structural components, or variations in crack shapes. The K relations for many different types of loading and specimen and crack geometries have been obtained by various experimental and analytical methods. Handbooks that give a variety of K relations are listed in the bibliography. These

9

handbooks give K relations for the three basic types of crack-face displacement shown in Fig. 4. Most crack-related fracture processes of practical significance for metals principally involve Mode I, opening-mode deformation, in which the displacement of the crack faces is in a direction perpendicular to the crack plane. There are cases in which shear deformation by Modes II and III accompanies opening-mode deformation, but shear deformation often has little significant effect on the over-all, **macroscopic** fracture process.

E. Fracture Toughness

Tests on precracked specimens of a wide variety of materials have shown that the critical K value at the onset of crack extension approaches a constant value as specimen thickness increases. Figure 5 shows this effect in tests with high-strength steel specimens over a range of thickness. In general, when the in-plane dimensions near the crack (i.e., crack length and uncracked ligament depth) are large compared to the size of the crack tip plastic zone (i.e., at least 15 times larger), Eq. 9 describing the linear elastic field may be considered to be valid. This is referred to as a state of small-scale yielding. In addition, if the out-of-plane specimen thickness exceeds $\sim$ 15 times the plastic zone size, then the value of K at which growth begins is a constant and generally minimum value called the plane-strain fracture toughness, K_{Ic}, of the material. The value of K_{Ic}

10

determined for a given material is unaffected by specimen dimensions or type of loading, provided that the specimen dimensions are large enough relative to the plastic zone to ensure plane-strain conditions around the crack tip (strain is zero in the through-thickness or z-direction).

Plane-strain fracture toughness, K_{Ic}, is directly related to the energy required for the onset of crack propagation by the formula:

$$K_{Ic} = \sqrt{EG_{Ic}/(1 - v^2)} \qquad (10)$$

where E is the elastic modulus (in MPa or psi), v is Poisson's ratio (dimensionless), and G_{Ic} is the critical plane-strain energy release rate for crack extension (in kJ/m^2 or $in.-lb/in.^2$). In simplified concept, G_{Ic} is the critical amount of strain energy that is released from the elastic stress field of the specimen per unit area of new cracked surface for the first small increment of crack extension. The concepts of K_{Ic} and G_{Ic} are essentially interchangeable; K_{Ic} is generally preferred because it is more easily associated with the stress or load applied to a specimen. The value of K_{Ic} for a given material can be measured directly using ASTM Standard Test Method E-399.

Plane-strain fracture toughness, K_{Ic}, is particularly pertinent in materials selection because, unlike other measures of toughness, it is independent of specimen configuration. In

11

selection of structural materials, the single most important characteristic of K_{Ic} for nearly all materials is that it varies inversely with yield strength. This is shown schematically in Fig. 6 using typical values from the published literature for high-strength steels. These data for steels are representative of the significant decrease in fracture toughness which occurs with an increase in yield strength for nearly all structural materials. It is easy to see that if materials for structural components are selected with only yield strength in mind, then the materials selector may be inviting the occurrence of a brittle, catastrophic fracture.

F. Role of Local Plasticity

When the stresses get sufficiently high near the crack tip, plastic deformation must occur. A description of the size of the plastic zone is essential to the understanding of how section size affects the fracture behavior of a specimen or component. The simplest concept is to imagine the point at which σ_{ij}, according to Eq. 9, reaches the yield strength of the material σ_0. This value of r represents the radius of the plastic zone (Fig. 3):

$$r_y\Big|_{\theta=0^\circ} \sim \frac{K_I^2}{2\pi\sigma_0^2} \qquad (11)$$

The actual size of the plastic zone depends upon the mode of applied loading, the geometry of the body and whether plane-strain

12

or plane-stress (stress is zero in the through-thickness direction) conditions apply. For a Poisson's ratio of $\nu = 0.3$, the average plane-strain plastic-zone size is about 1/3 the plane-stress value of Eq. 11, considering all values of θ. The important point is that yielding in thick plates is more difficult, the plastic zones are smaller, and hence the energy absorbed around the crack is less.

G. Nonlinear Elastic Fracture Mechanics

Fracture mechanics is generally applied to describe the crack-growth process for a number of test and service conditions in addition to those of plane-strain, K_{Ic}-type fracture. The main additional categories of crack growth are elastic-plastic crack growth, fatigue crack growth, and crack growth as affected by testing environment in the general sense -- that is, chemical environment, temperature and loading rate.

For cracked and loaded specimens of relatively low-strength materials and relatively small section sizes, the size of the plastic zone at the crack tip can be significant relative to the section size. When this occurs, the assumption that the elastic stress around the crack controls the fracture process is no longer valid, and the conditions around the crack may represent plane stress (strain is nonzero in the z-direction). Furthermore, crack growth generally occurs with a shear-lip type of deformation near

13

external surfaces, resulting in a critical value of K which is higher than that for elastic-stress-controlled crack growth.

Where the in-plane specimen dimensions are still large compared to the plastic zone size, but the sheet thickness is insufficient for plane-strain conditions to apply, the resistance-curve or R-curve approach is generally used. Briefly, the resistance-curve concept involves measurement of the K values at which various amounts of crack growth occur in a thin-plate laboratory specimen. Then a plotted curve of K versus crack growth from the laboratory specimen can be used to predict crack-growth behavior in a structural component of the same material. Limitations of the method are that the component must have the same thickness as the laboratory specimen and that K relations must be known for both component and specimen. However, once a resistance curve is obtained for a given material and thickness, it can be used to predict the crack-growth and crack-instability behavior of other components of the same material.

Where the extent of plasticity becomes large compared to the in-plane specimen dimensions as well (referred to as large-scale yielding) an alternative characterizing parameter approach must be used, based on elastic-plastic (or more correctly nonlinear elastic fracture mechanics). For a material obeying the constitutive law where the uniaxial stress σ is related to the uniaxial plastic strain ϵ_p by:

14

$$\frac{\epsilon_p}{\epsilon_0} = \alpha \left(\frac{\sigma}{\sigma_0} \right)^n \tag{12}$$

where σ_0 and ϵ_0 are the yield stress and strain, n is the work-hardening exponent and α is a material constant of order unity, the asymptotic form of the local stress, strain and displacement nonlinear elastic fields is given, as $r \to 0$, by:

$$\sigma_{ij} \to \sigma_0 \left[\frac{J}{\alpha \, \sigma_0 \, \epsilon_0 \, I_n \, r} \right]^{\frac{1}{n+1}} \tilde{\sigma}_{ij}(\theta, n)$$

$$\epsilon_{ij} \to \alpha \epsilon_0 \left[\frac{J}{\alpha \, \sigma_0 \, \epsilon_0 \, I_n \, r} \right]^{\frac{n}{n+1}} \tilde{\epsilon}_{ij}(\theta, n)$$

$$u_i \to \alpha \epsilon_0 r \left[\frac{J}{\alpha \, \sigma_0 \, \epsilon_0 \, I_n \, r} \right]^{\frac{n}{n+1}} \tilde{u}_i(\theta, n) \tag{13}$$

where I_n is a dimensionless integration constant (given approximately by $I_n = 10.3\sqrt{0.13 + n} - 4.8\,n$), $\tilde{\sigma}_{ij}$, $\tilde{\epsilon}_{ij}$ and $\tilde{u}_i$ are normalized stress, strain and displacement functions of θ and n, and J is the so-called path-independent J-integral. The amplitude of this field is the J-integral, and analogous to K_I in Eq. 9, J uniquely and autonomously characterizes the crack tip field under elastic-plastic conditions **provided some degree of strain-hardening exists.** Further, for small-scale yielding, J can be directly related to the strain energy release rate G, and hence K_I, i.e.:

$$J = G = K_I^2/E' \qquad \text{(linear elastic)} \tag{14}$$

15

In essence, J can be thought of as the amount of elastic-plastic strain energy per unit area of crack growth which is applied toward extending the crack in a specimen under load. A critical value of J, called J_{Ic}, is the value required for the start of crack extension from a pre-existing crack. For material having a sufficiently high yield strength or for specimens of sufficient size, elastic stresses control the crack extension, and J_{Ic} is equal to G_{Ic}.

The great advantage of the J_{Ic} approach is that it makes possible the prediction of the failure load of a cracked component or the measurement of the fracture toughness of a material even when there is significant plastic deformation present in the component or material sample. This is an important advantage because, in recent years, high-toughness, medium-strength alloys (with more tendency toward plastic deformation) have been used in place of high-strength, low-toughness alloys for many fracture-critical applications. Details of the J_{Ic} method to estimate the fracture toughness of a material are given in the ASTM Standard Test Method E813. As with K_{Ic}, the J_{Ic} method uses precracked specimens of fixed geometry and of a minimum required size. The size requirement allows the use of smaller specimens than the K_{Ic} test, so fracture toughness measurements are possible using J_{Ic} for materials and sizes which are outside the range of the K_{Ic} method.

An alternative approach to elastic-plastic crack growth is to utilize the concept of crack tip opening displacement (CTOD). From

16

Eq. 13, it is apparent that the opening of the crack faces at $r \to 0$ varies as $r^{\frac{1}{(n+1)}}$, such that this separation can be used to define the CTOD (δ_t) as the opening where 45° lines emanating back from the crack tip intercept the crack faces, i.e.:

$$\delta_t = d(\epsilon_0,n) \frac{J}{\sigma_0^2} \qquad \text{(elastic-plastic)}$$

$$\propto \frac{K_I^2}{\sigma_0 E'} \qquad \text{(linear elastic)} \qquad (15)$$

where d is a proportionality factor (~ 0.3 to 1) dependent upon the yield strain ϵ_0, the work—hardening exponent n, and whether plane-stress or plane—strain is assumed. Since δ_t, like J, can be taken as a measure of the intensity of the elastic-plastic crack tip fields, it is feasible to correlate crack initiation and growth to the crack opening displacement.

Approaches based on J and δ_t are basically equivalent for proportional loading, and are of course valid under both elastic-plastic and linear elastic conditions. Therefore, they are generally applicable to a continuum description of the growth-rate behavior of cracks considered small because their size is comparable with the scale of local plasticity.

17

II. MICROSCOPIC APPROACH TO FRACTURE

A. Micromechanisms

Since macroscopic fracture criteria, such as those based on K_I or J, result from the asymptotic continuum mechanics characterization, realistic evaluation of toughness using K_{Ic} or J_{Ic} does not necessitate any microscopic understanding of the fracture events involved. However, in the interest of a full comprehension of a fracture process and specifically to define which microstructural features contribute to a material's toughness, it is often beneficial to construct microscopic models for specific fracture mechanisms. Such models are generally referred to as "micromechanisms." Unlike the continuum approach, this requires a microscopic model for the particular fracture mode, which incorporates a local failure criterion and consideration of salient microstructural features, as well as detailed knowledge of both the asymptotic and very-near tip stress and deformation fields. Physical fracture processes, and consequently the local failure criterion and characteristic microstructural dimensions, vary substantially, however, with fracture mode, as Fig. 7 illustrates for the four classical fracture morphologies, i.e., microvoid coalescence, quasi-cleavage, intergranular, and transgranular cleavage.

18

B. Ductile Fracture

Microvoid coalescence (Fig. 7a) is the process by which slow stable tearing crack growth and unstable ductile fracture occurs. It involves the nucleation of voids, generally by interface decohesion between second-phase particles and the matrix, or by actual cracking of particles, their growth and eventual coalescence to form a macroscopic crack. The size and spacing of the particles clearly are important (generally larger, closely spaced particles are detrimental), and also the mode of coalescence. In low strain-hardening materials, or in the presence of smaller particles or dispersoids, the linkage of major voids occurs prematurely by strain localization along shear bands of small voids nucleated at the smaller particles.

This fracture mechanism can be modelled in order to estimate the fracture toughness of a material failing by void coalescence. At crack initiation at $J = J_{Ic}$, it is assumed that the local equivalent strain $\bar{\varepsilon}_p$ at the crack tip (from Eq. 13) exceeds a critical fracture strain $\bar{\varepsilon}_f^*$, appropriate to the triaxial conditions near the tip, over a characteristic microstructural distance ℓ_0^*, comparable with the mean particle spacing d_p (Fig. 8b). By simplifying the strain distribution in Eq. 13 by assuming large $n \sim 10$, and by applying this criterion of $\bar{\varepsilon}_p$ exceeding $\bar{\varepsilon}_f^*$ over $r = \ell_0^*$ at $J = J_{Ic}$, the ductile fracture toughness can be expressed as:

19

$$K_{Ic} \sim \sqrt{E \, \sigma_0 \, \bar{\epsilon}_f^* \, \ell_0^*}$$

or

$$J_{Ic} \sim \sigma_0 \, \bar{\epsilon}_f^* \, \ell_0^* \qquad (16)$$

Thus, for ductile fracture, toughness is proportional to strength times ductility. Eq. 16 also permits the rationalization of the toughness-strength relation (Fig. 6) for cases where microstructural changes which increase strength also cause a more rapid reduction in ductility.

The ductility itself can be estimated by considering an array of void-initiating particles, of diameter D_p and mean spacing d_p, and allowing them to grow in a triaxial field ahead of a crack until they impinge, thus:

$$\bar{\epsilon}_f^* \sim \frac{\ell n(d_p/D_p)}{0.28 \, \exp(1.5 \, \sigma_m/\bar{\sigma})} \qquad (17)$$

where $\sigma_m/\bar{\sigma}$ is the ratio of hydrostatic to equivalent stress and defines the degree of triaxiality. Although this analysis considers the fracture strain to be limited by the simple impingement of the growing voids and thus tends to overestimate $\bar{\epsilon}_f^*$ by ignoring prior coalescence due to shear banding by strain localization, it correctly suggests a dependence of $\bar{\epsilon}_f^*$ on stress state $(\sigma_m/\bar{\sigma})$, and purity (d_p/D_p). For example, a large effect of stress state (i.e., triaxiality) on fracture strain is predicted such that from Eq. 17, $\bar{\epsilon}_f^*$ would be expected to be reduced by an

20

order of magnitude by going from an unnotched plane-strain condition to that ahead of a sharp crack. The benefits of increased purity (i.e., increased particle spacing d_p), however, are pronounced only at low D_p/d_p ratios due to the logarithmic terms in Eq. 17. For example, reducing the volume fraction f_p of inclusions from 0.001 to 0.000001 would increase $\bar{\varepsilon}_f^*$ only by a factor of 2.

C. Brittle Fracture

At low temperatures or in very high-strength material, microcracks initiated at particles, interfaces or at general inhomogeneities in the material, are unable to blunt plastically. In these cases, brittle fracture may ensue, either by the transgranular cleavage of grains on low energy crystallographic planes (Fig. 7b and d) or by intergranular cracking along the grain boundary surfaces. Many materials, like steels, show a ductile-brittle transition. They fail by cleavage at low temperature, where their yield strength is high, and show a low toughness, whereas due to softening at higher temperature, their toughness is considerably higher as failure occurs by void coalescence. When designing with such materials, it is vital to know which regime the material will experience in service.

Modeling brittle fracture can be achieved in a similar fashion to that of ductile fracture. Here at crack initiation, $K_I = K_{Ic}$, a stress-controlled criterion is assumed whereby the local <u>tensile</u>

21

stress (from Eq. 13) exceeds a critical fracture surface, σ_f^*, over a microstructurally-significant dimension comparable with the grain size, $\ell_0^* \sim d_g$ (Fig. 8a). This implies a brittle fracture toughness of:

$$K_{Ic} \sim \left(\frac{\sigma_f^{* \frac{n+1}{2}}}{\sigma_0^{\frac{n-1}{2}}} \right) \ell_0^{* \frac{1}{2}} \qquad (18)$$

In steels, with ferrite/carbide microstructures, the characteristic distance has been found to be on the order of the spacing of the void initiating grain boundary carbides, i.e., typically $\sim$ two grain diameters (d_g), although different size scales have been identified when the analysis is applied to other materials. The model has been found to be particularly successful both in quantitatively predicting cleavage fracture toughness values in a wide range of microstructures and furthermore in rationalizing the influence on K_{Ic} of such variables as temperature, strain rate, neutron irradiation, warm prestressing, and so forth. Somewhat similar microscopic models involving a critical stress criterion have been suggested for other fracture modes, including intergranular cracking (Fig. 7c) in temper-embrittled steels and hydrogen-assisted fracture.

The success of the microscopic models for predicting fracture toughness can be appreciated in Fig. 9 where the critical-stress

22

model for cleavage and the critical-strain model for ductile
fracture are utilized to predict the respective lower and upper
shelf toughness in ASTM A533B-1 nuclear-pressure-vessel steel.
Whereas the characteristic distance (ℓ_0^*) for cleavage fracture
scales approximately with 2 to 4 times the grain size (essentially
the bainite packet size), for ductile fracture ℓ_0^* was found to be
approximately five to six times the average major inclusion spacing
(d_p).

D. Intrinsic vs. Extrinsic Toughening

In fracture mechanics terms, the extension of a crack can be
considered to be driven by the presence of a **"crack driving force"**
and opposed by the **resistance of the microstructure.** Here the
driving force is defined by the stress intensity K_I or J-integral,
which describes the dominant stress and deformation fields in the
vicinity of the crack tip from a knowledge of crack size, applied
load and geometry. By similitude, cracks are then assumed to
extend at equal rates when subjected to equal "driving forces."
Crack advance is thus restrained by lowering the applied load or by
"toughening" the material, e.g., impeding crack growth through
compositional or microstructural modification.

The toughening models described above represent situations
where resistance to crack growth is achieved by increasing the
inherent microstructural resistance, e.g., by coarsening particle
spacings, increasing ductility, etc.; a process termed **intrinsic**

23

toughening. Most metals derive their toughness by such mechanisms (Table 1). However, in many material systems, e.g., cracking in ceramics, rocks and fiber composites, the actual source of toughness may be distinctly different, arising from mechanisms of **crack tip shielding.** Here crack extension is impeded, by mechanical, microstructural and environmental factors which locally reduce the crack driving force; a process termed **extrinsic toughening.** The various mechanisms of shielding are shown in Fig. 10.

In ceramics, for example, the intrinsic toughness of zirconia is a mere 2 MPa$\sqrt{m}$. However, by inducing an in situ phase transformation at the crack tip (transformation toughening) or by causing the in situ microcracking of particles (microcrack toughening),both processes causing a dilation around the crack tip which is constrained by surrounding elastic material, the measured toughness can be raised extrinsically to between 8 and 14 MPa$\sqrt{m}$ (Table 1). Similarly, by inducing crack branching and meandering, due to crack deflection at particles or interfaces, factors of 3 increases in toughness can be obtained. Composites can be also toughened by such mechanisms. A potent form of crack tip shielding in these materials is through crack briding (ligament toughening), where, for example, the crack is made to intersect a ductile fiber which undergoes plastic deformation as the crack passes.

24

Table 1 Strength and Fracture Toughness Data for Typical Metals, Ceramics, Polymers and Composites

Material	Yield Strength σ_o (MPa)	Fracture Toughness K_{Ic} (MPa$\sqrt{m}$)	Plastic Zone Size r_y (μm)
Metals			
4340 Steel 200°C Temper	1700	60	200
Maraging Steel	1450	110	920
A533B-1 Mild Steel	500	245	4×10^4
7075-T651 Aluminum Alloy	515	28	470
2024-T351 Aluminum Alloy	370	35	1420
Ti-6Al-4V Titanium Alloy	850	120	3170
Ceramics			
Glass	1700*	0.8	0.04
Silicon Carbide	7000*	3.0	0.03
Zirconia	4300*	2.0	0.03
Partially Stabilized Zirconia	4000*	14.0	2
Tungsten Carbide	4000*	10.0	1
Polymers			
Polycarbonate	70	3.0	290
PMMA	-	1.5	-
Composites			
SiC in Glass	-	20	-
15 wt% Co in Tungsten Carbide	3500*	18	4

*Estimated from hardness data

25

Due to the high degree of crack tip blunting, extrinsic toughening is less important in metals. However, at low stress intensities during sub-critical crack growth, crack tip shielding can play a dominant role in metallic materials, such as with the wedge shielding mechanisms (crack closure) during fatigue crack growth (Section III).

III. FATIGUE CRACK PROPAGATION

A. Background

Crack growth can occur at K levels much below K_{Ic} in any structural alloy when cyclic loading is applied. In simplified concept, it is the accumulation of damage from the cyclic plastic deformation in a small zone at the crack tip which accounts for fatigue crack growth at K levels much below K_{Ic}.

Fatigue represents the principal cause of in-service failures of engineering structures and components, whether associated with mechanical sliding or friction (fretting fatigue), aggressive environments (corrosion fatigue) and elevated temperatures (creep-fatigue). The process of fatigue failure itself consists of several distinct processes involving initial cyclic damage (cyclic hardening or softening), formation of an initial "fatal" flaw (crack initiation), macroscopic propagation of this flaw (crack growth) and final catastrophic failure or instability.

26

The physical phenomenon of fatigue was first seriously considered in the mid-nineteenth century when widespread failures of railway axles in Europe prompted Wohler in Germany and Fairbairn in England to conduct the first systematic investigations into the fracture of materials under cyclic stresses circa 1860. Somewhat later, in 1917, the first reported observations of corrosion-fatigue were made by Haigh concerning the effect of sea-water on the failure of steel cables. However, the main impetus for research directed at the crack propagation stage of fatigue failure, as opposed to mere lifetime calculations, did not occur until the mid-1960's when the concepts of linear elastic fracture mechanics and so-called "defect-tolerant design" were first applied to the problem of sub-critical flaw growth. Such approaches recognize that all structures are flawed, and that cracks may initiate early in service life and propagate sub-critically. Lifetime is then assessed on the basis of the time or number of loading cycles for the largest undetected crack to grow to failure, as might be defined by an allowable strain, or limit load or fracture toughness (K_{Ic}) criterion. Implicit in such analyses is that sub-critical crack growth can be characterized in terms of some governing parameter (often thought of as a crack driving force) which describes local conditions at the crack tip yet may be determined in terms of loading parameters, crack size and geometry. Linear elastic and nonlinear elastic fracture mechanics have, to

27

date, provided the most appropriate methodology for such analyses
to be made.

B. Fracture Mechanics Characterization of Fatigue Crack Growth

The general nature of fatigue crack growth and its description
using fracture mechanics can be briefly summarized by the schematic
diagram shown in Fig. 11. This figure shows a logarithmic plot of
the increment of fatigue crack extension (da/dN), each cycle, as a
function of the range of nominal stress intensity, given by the
difference in the maximum and minimum stress intensities over the
cycle ($\Delta K = K_{max} - K_{min}$). A plot of similar shape is expected with
most structural alloys. Results of fatigue crack growth rate tests
for nearly all metallic structural materials have shown that the
da/dN versus ΔK curves have the following characteristics: (a) a
region at low values of da/dN and ΔK in which fatigue cracks grow
extremely slowly or not at all below a lower limit of ΔK called the
threshold of ΔK, ΔK_{TH}; (b) an intermediate region of power-law
behavior described by the Paris equation:

$$da/dN = C(\Delta K)^m \qquad (19)$$

where C and m are material scaling constants; and (c) an upper
region of rapid, unstable crack growth with an upper limit of ΔK
which corresponds either to K_{Ic} or to gross plastic deformation of
the specimen. Similar approaches have been suggested for crack

28

growth under large-scale yielding where growth rates are related to ΔJ or $\Delta CTOD$. Typical data can be seen in Fig. 12 for a 7150 aluminum alloy (Al-6 wt% Zn, 2 wt% Mg, 2 wt% Cu) tested at load ratios ($R = K_{min}/K_{max}$) of 0.10 and 0.75.

C. Experimental Measurement

Fatigue crack propagation rate data are generally measured using standard fracture mechanics-type specimen geometries, such as the compact tension, edge-notched bend, or center-cracked sheet test pieces. Starting from a mechanically sharpened crack, specimens are subjected to a cyclically varying load ΔP, generally under constant load control (increasing stress intensity K_I), and the increase in crack length monitored (as a function of time or number of cycles N at constant frequency) using such techniques as travelling microscopes, high-speed photography, compliance measurements, ultrasonics or acoustic-emission detectors or electrical resistivity measurements, gauges or crack mouth displacement gauges, and ultrasonic or acoustic emission detectors. Data are used to construct crack length (a) versus number of cycles (N) plots, which are then differentiated, either graphically or numerically, to determine the rate of crack growth $(da/dN)_{a_i}$ for each crack length a_i (Fig. 13). Corresponding to each crack length a_i, the value of $(\Delta K)_{a_i}$ is computed from the applied loads and the relevant K_I calibration for the particular test geometry, such that the data are finally presented in the form of log-log plots of

29

da/dN versus ΔK (Fig. 12). Empirical expressions, of the form of Eq. 19, are then numerically fitted to the data to define the crack growth relationship (e.g., Eq. 19) for the particular combination of material, testing conditions, and environment in question. These procedures have now been standardized in ASTM Standard Test Method E647-81.

At very low crack propagation rates, below typically 10^{-6} mm/cycle, it is generally necessary to monitor growth rates under load-shedding (decreasing ΔK) conditions in order to determine the fatigue threshold ΔK_{TH}, below which cracks appear to be dormant.

Such fatigue crack-growth measurement procedures can be easily automated using a suitable crack monitoring technique and a computer-controlled testing machine. This is particularly relevant for near-threshold testing under load-shedding conditions, where a programmed constant decrease in the normalized K_I gradient, i.e., $|\Delta K^{-1} \cdot d\Delta K/da|$, can be utilized.

D. Microstructural Characteristics of Fatigue Crack Growth

Fatigue failure is generally characterized by a transgranular ductile striation mechanism, as shown in Fig. 14a. Such striations represent local crack-growth increments per cycle, and have been hypothesized to occur via a mechanism of opening, advancing and blunting of the crack tip on loading, followed by resharpening of the tip on unloading. Several theoretical models for such growth (often termed Stage II crack propagation) have been proposed which

30

rely on the fact that, where plastic zones are sufficiently large compared to microstructural dimensions, plastic blunting at the crack tip is accommodated by shear on two slip-systems roughly 45° to the crack plane. Recognizing that such sliding-off is largely irreversible, new crack surface can be created during cyclic crack advance either by simultaneous or alternating slip on these two systems.

Such models predict that an upper bound estimate for the increment of crack advance per cycle should be proportional to the cyclic crack tip opening displacement (ΔCTOD), viz:

$$\frac{da}{dN} \propto \Delta\text{CTOD} \sim \beta \frac{\Delta K^2}{2\sigma_0 E} \tag{20}$$

where β is a proportionality constant, of order 0.1 to 1, reflecting the efficiency of crack tip blunting.

At high fatigue crack growth rates, typically above $\sim 10^{-3}$ mm/cycle, where K_{max} approaches K_{Ic} or limit load failure (regime C in Fig. 11), the Paris law (Eq. 19) generally underestimates measured growth rates due to the occurrence of brittle fracture mechanisms (so-called static modes) which replace or are additional to striation growth. Such static modes include cleavage, intergranular cracking and microvoid coalescence (Fig. 14) and their presence results in growth rate behavior which is markedly sensitive to microstructure, load ratio and test piece thickness. Conversely, at very low growth rates below $\sim 10^{-6}$ mm/cycle

31

approaching the fatigue threshold ΔK_{TH} (regime A in Fig. 11), the Paris law (Eq. 19) generally overestimates measured growth rates and behavior becomes markedly sensitive to mean stress, microstructure and environment. In addition, at such near-threshold levels, the scale of local plasticity approaches microstructural size-scales, and measured growth rates become less than an interatomic spacing per cycle, indicating that crack advance is not occurring uniformly over the entire crack front. Crack growth mechanisms in this regime generally are faceted, often being referred to as "microstructurally-sensitive" or "crystallographic" fatigue, and reflect more of a shear mode of crack advance with associated Mode II + Mode I displacements, particularly in coarse planar slip materials. Behavior in this regime is again markedly sensitive to microstructure and load ratio, and, because growth rates are so slow, to the environment.

E. Fatigue Crack Closure

Implicit in the analyses of fatigue crack propagation so far, it has been assumed that the full range of ΔK, computed on the basis of $K_{max} - K_{min}$ from applied loads and crack length measurements, is available as the nominal driving force for crack extension. However, should physical contact between the mating crack surfaces occur at positive loads during the fatigue cycle as a result of the local deformation and fracture processes, this driving force would be effectively limited at the crack tip. Such

32

contact between fatigue crack surface is another form of crack tip shielding (Fig. 10), and is referred to as crack closure.

As envisioned by Elber, crack closure, or more precisely **plasticity-induced crack closure**, can be considered to occur from interference between crack surfaces in the wake of the crack tip, arising from the constraint of surrounding elastic material on the residual stretch in material elements previously plastically-strained at the tip. Since the crack cannot propagate whilst it remains closed, the net effect of this closure is to reduce the nominal stress intensity range ΔK to some lower effective value ΔK_{eff} actually experienced at the crack tip, i.e.:

$$\Delta K = K_{max} - K_{min} \qquad \text{(no closure)}$$
$$\Delta K_{eff} = K_{max} - K_{cl} \qquad \text{(with closure)} \qquad (21)$$

where K_{cl} is the stress intensity to close the crack ($\geq K_{min}$) (Fig. 15).

There are several other mechanisms of crack closure which assume greater importance at near-threshold stress intensities, where crack opening displacements are small. These closure processes generally rely on wedging mechanisms inside the crack, either by corrosion debris, fracture surface asperities, or, in the case of environmentally-assisted fatigue, by fluid inside the crack (Fig. 10).

33

Crack closure arising from crack surface corrosion deposits, referred to as **oxide-induced closure**, is promoted in oxidizing environments at low load ratios. Notable examples are the crack surface oxides and calcareous deposits formed during corrosion fatigue in structural steels tested, respectively, in water and seawater, and the chromic oxides formed during creep-fatigue in Ni-based superalloys. Simple quantitative modelling, based on the concept of a rigid wedge inside a linear elastic crack, suggests that such closure depends upon the thickness, s, of the oxide film and the location of its peak thickness from the crack tip, 2z, i.e.:

$$K_{cl} \sim \frac{s\,E}{4\sqrt{\pi z}\,(1 - \nu^2)} \tag{22}$$

implying that deposits in the immediate vicinity of the crack tip will have a dominating influence in the development of closure by this mechanism.

In lower-strength materials, particularly in low carbon steels, the extent of the corrosion debris can be significantly enhanced at low load ratios from fretting oxidation processes between the crack walls. This can produce surprising results, such as observations in alloy steels of near-threshold growth rates being significantly faster in dry helium gas, and slower in water or steam, compared to behavior in room air. Since susceptibility to hydrogen embrittlement is not large in these steels, such

34

results simply can be interpreted in terms of less corrosion deposits being generated in the dry atmospheres. With steels of higher strength and in many aluminum alloys, the degree of fretting oxidation between crack surfaces appears much reduced with the result that the contribution from this mechanism becomes negligible.

A more general source of closure arises from the wedging action of fracture surface asperities, where crack tip opening displacements are small and where significant Mode II crack tip shear displacements occur. Such **roughness-induced closure** is promoted at near-threshold levels, particularly where crack advance is strongly crystallographic, as in coherent-particle-hardened (planar slip) systems such as underaged aluminum alloys and Ni-based superalloys or in duplex microstructures where the crack can be made to meander from frequent crack deflection (Fig. 16). Notable examples of where crack deflection and the resulting roughness-induced closure has led to significant reductions in crack growth rates can be found for dual-phase steels, β-annealed titanium alloys and aluminum-lithium alloys.

The magnitude of roughness-induced mechanism depends upon the degree of fracture surface roughness and the extent of the Mode II crack tip displacements. From simple two-dimensional geometric modelling, the closure stress intensity at the point of first asperity contact has been derived to be:

$$K_{cl} \sim \sqrt{\frac{2\gamma u}{1 + 2\gamma u}} \cdot K_{max} \qquad (23)$$

where γ is a measure of surface roughness, i.e., ratio of height to width of the asperities, and u is the ratio of Mode II to Mode I displacements.

F. Small Fatigue Cracks

Crack closure mechanisms can exert a strong retarding influence on fatigue crack propagation, particularly at near-threshold levels. Moreover, they account for strong load ratio effects, decreased growth rates in coarse planar slip or duplex microstructures, and for so-called "small crack" effects. The latter phenomenon follows because, in common with all crack tip shielding mechanisms, crack closure acts upon the crack wake. If this wake is restricted, such as with cracks which are small compared to the scale of microstructure or local plasticity, or are simply physically small (i.e., < 1 mm), then the effect of closure is lessened. Consequently, the local 'driving force,' i.e., ΔK_{eff}, experienced by a small crack may be significantly larger than that experienced by a larger crack (> 10 mm) at the same nominal ΔK level. This is the primary reason why small cracks behave in "anomalous" fashion in growing below the fatigue threshold ΔK_{TH}, and in general propagating at rates in excess of those of long cracks (Fig. 17).

G. Variable Amplitude Loading

A further consequence of crack closure is the load interaction effects observed during variable amplitude loading. Since the majority of components in service are subjected to variable-amplitude, spectrum or random loading, rather than constant-amplitude loading, an appreciation of the influence of periodic overloads and block loading sequences on fatigue crack propagation is clearly of practical significance. Classically, the approach taken for variable-amplitude loading in fatigue design is to use the Palmgren-Miner relationship, where for a body subjected n_i number of cycles of different stress amplitudes $\Delta\sigma_{a_i}$, with i = 1 to k:

$$\sum_{i=1}^{k} \frac{n_i}{N_i} = 1 \qquad (24)$$

where N_i is the number of cycles-to-failure had all the stress amplitudes been of magnitude $\Delta\sigma_{a_i}$. This approach, which is utilized for **total** life prediction and thus includes both crack initiation and crack propagation stages, predicts that the cycles-to-failure will be decreased if a large single positive (spike) overload is applied during constant amplitude cycling. However, as shown in Fig. 18 for a titanium alloy, the effect of such an overload on Mode I crack propagation rates is to retard crack growth initially, sometimes to the point of arrest, and thus to increase the **propagation** life. Hence it is apparent that the

37

application of Miner's rule to crack propagation behavior under variable amplitude loads is generally inappropriate.

For crack growth studies, however, the above approach can be utilized for narrow-band random loading where each cycle does not differ significantly from its predecessor. Here interaction effects can be considered small and it is reasonable to assume that each cycle causes the same amount of crack extension as if it were applied as part of a sequence of constant amplitude loads. For broad-band loading, on the other hand, cyclic crack extension has been estimated on the basis that the load, or stress intensity, ranges are constant at their root mean square value. However, since loading sequence interaction effects are more relevant here, this procedure often yields conservative predictions for crack advance.

The nature of these interaction effects is shown in Fig. 18. The application of a single positive (spike) overload of sufficient magnitude (generally > 50% of the baseline ΔK) can result in significantly retarded crack growth over a crack length increment which is of the order of, or greater than, the overload plastic zone size, whereupon crack growth rates return to their original baseline level. Sometimes cracks overloaded in this fashion totally arrest, where presumably the effective stress intensity actually experienced at the crack tip is reduced below ΔK_{TH}. However, the onset of the retardation or crack arrest often does not coincide with the actual overload cycle but is delayed until

38

the crack has grown some distance into the overload plastic zone (so-called delayed retardation). For fully reversed overload cycles, the application of an underload (compressive overload) prior to a single overload does not appear to have much effect on subsequent retardation, whereas an underload following an overload tends to minimize retardation. Block loading sequences are also known to produce large transient effects on fatigue crack propagation.

The origin of load interaction effects is still somewhat unclear, but following a single tensile overload for example, the crack is retarded due to blunting and crack growth into the residual compressive stress field of the overload plastic zone. This in turn induces additional crack closure, from both the plasticity and roughness mechanisms, in the wake of the crack tip, which prolongs the period of retardation.

IV. ENVIRONMENTALLY-INFLUENCED FRACTURE

There are countless combinations of physical and chemical testing environments which can affect crack growth in structural alloys. For a few conditions, an increase in the stress intensity is required for crack growth at a designated rate, but generally cracking can be induced to occur at lower stress intensities when specimens are exposed to service environments other than normal laboratory air. The mechanisms of crack growth that can occur with

various testing environments are too numerous and complex for discussion here. However, the general variations in testing environment can include variations in testing temperature, rate of loading, and chemical environment. For these three types of variations, fracture tests generally can be performed using laboratory specimens of the same or similar types as those used for testing under normal conditions.

As with fatigue crack propagation, results of sustained loading may be shown in logarithmic plots of crack growth rate versus applied K -- except with da/dt being plotted instead of da/dN. Results of sustained-load tests on specimens of 4340 alloy steels immersed in distilled water to develop stress-corrosion cracking are shown in Fig. 19. Both crack-mouth-opening-displacement and traveling-microscope techniques were used to measure crack growth rates, because the relatively low velocities permit direct measurement of crack length during the out-of-solution period. These results are typical, and they show that as K is increased from some threshold value, the subcritical crack velocity increases by several orders of magnitude. A plateau region is then reached where velocity is relatively independent of K but dependent on temperature. As might be expected, temperature generally enhances the kinetics of environmental attack and diffusion of embrittling species, so growth rates increase at higher temperatures. Finally, if growth rates had been measured at

K values closer to K_{Ic}, the crack velocities would have increased dramatically as K_{Ic} was approached.

The major difficulty and limitation of measuring crack growth as affected by testing environment is in accurately producing and maintaining the specified test conditions during the laboratory test. The proper use of high and low loading rates, high-and low-temperature chambers, and chemical environment chambers can greatly increase the time and cost required to obtain laboratory test results. Nevertheless, test results for various service conditions are required in order to apply fracture mechanics to the selection of materials and thereby to avoid the catastrophic failures which can occur in components and structures which are adversely affected by service environments.

BIBLIOGRAPHY

Anon, <u>ASTM Annual Book of Standards</u>, American Society for Testing and Materials, Philadelphia, PA, 1986.

Broek, D., <u>Elementary Engineering Fracture Mechanics</u>, Martinus Noordhoff, The Hague, 3rd edition, 1982.

Elber, W., <u>Damage Tolerance in Aircraft Structures</u>, ASTM STP 486, American Society for Testing and Materials, p. 230, 1971.

Evans, A. G. and Faber, K. T., <u>Journal of American Ceramics Society</u>, vol. 67, p. 256, 1984.

Gangloff, R. P. and Wei, R. P., <u>Small Fatigue Cracks</u>, R. O. Ritchie and J. Lankford, eds., TMS-AIME, Warrendale, PA, p. 239, 1986.

Gerberich, W. W. and Moody, N. R., in <u>Fatigue Mechanisms</u>, ASTM STP 675, American Society for Testing and Materials, p. 292, 1979.

Griffith, A. A., <u>Philosophical Transactions</u>, vol. 221, p. 163, 1921.

Hellen, K., <u>Introduction to Fracture Mechanics</u>, McGraw-Hill, 1984.

Hertzberg, R. W. <u>Deformation and Fracture Mechanics of Engineering Materials</u>, Wiley, N.Y., 2nd ed., 1983.

Hutchinson, J. W., <u>Journal of Mechanics and Physics of Solids</u>, vol. 16, p. 13, 1968.

Irwin, G. R., <u>Journal of Applied Mechanics</u>, vol. 24, p. 361, 1957.

Knott, J. F., <u>Fundamentals of Fracture Mechanics</u>, Butterworths, London, 1973.

Landes, J. D. and Begley, J. A., Developments in Fracture Mechanics Test Methods Standardization, ASTM STP 632, American Society for Testing and Materials, 1977.

Lankford, J., Fatigue and Fracture of Engineering Materials and Structures, vol. 8, p. 161, 1985.

Mackenzie, A. C., Hancock, J. W. and Brown, D. K., Engineering Fracture Mechanics, vol. 9, p. 167, 1977.

McClintock, F. A., Fundamental Aspects of Structural Alloy Design, R. I. Jaffee and B. A. Wilcox, eds., Plenum, New York, p. 147, 1977.

McMeeking, R. M. and Evans, A. G., Journal of American Ceramics Society, vol. 65, p. 242, 1982.

Pelloux, R. M. N., Engineering Fracture Mechanics, vol. 1, p. 647, 1970.

Paris, P. C. and Erdogan, F., Journal of Basic Engineering, Transactions of ASME, vol. 85, p. 528, 1983.

Rice, J. R., Fracture: An Advanced Treatise, H. Liebowitz, ed., Academic Press, N.Y., vol. 2, p. 191, 1968.

Rice, J. R., Journal of Applied Mechanics, vol. 35, p. 379, 1968.

Rice, J. R. and Rosengren, G. R., Journal of Mechanics and Physics of Solids, vol. 16, p. 1, 1968.

Rice, J. R. and Tracey, D. M., Journal of Mechanics and Physics of Solids, vol. 17, p. 201, 1969.

Ritchie, R. O., Knott, J. R. and Rice, J. R., Journal of Mechanics and Physics of Solids, vol. 21, p. 395, 1973.

Ritchie, R. O. and Thompson, A. W., Metallurgical Transactions A, vol. 16A, p. 233, 1985.

Ritchie, R. O. and Yu, W., Small Fatigue Cracks, R. O. Ritchie and J. Lankford, eds., TMS-AIME, Warrendale, PA, p. 167, 1986.

Rolfe, S. T. and Barsom, J. M., Fracture and Fatigue Control in Structures, Prentice-Hall, Englewood Cliffs, NJ, 1977.

Suresh, S. and Ritchie, R. O., International Metals Reviews, vol. 29, p. 445, 1984.

Suresh, S and Ritchie, R. O., in Fatigue Crack Growth Threshold Concepts, D. L. Davidson and S. Suresh, eds., TMS-AIME, Warrendale, PA, p. 227, 1984.

Tada, H., Paris, P. C. and Irwin, G. R., The Stress Analysis of Cracks Handbook, Del Research Corporation, Hellertown, PA, 1973.
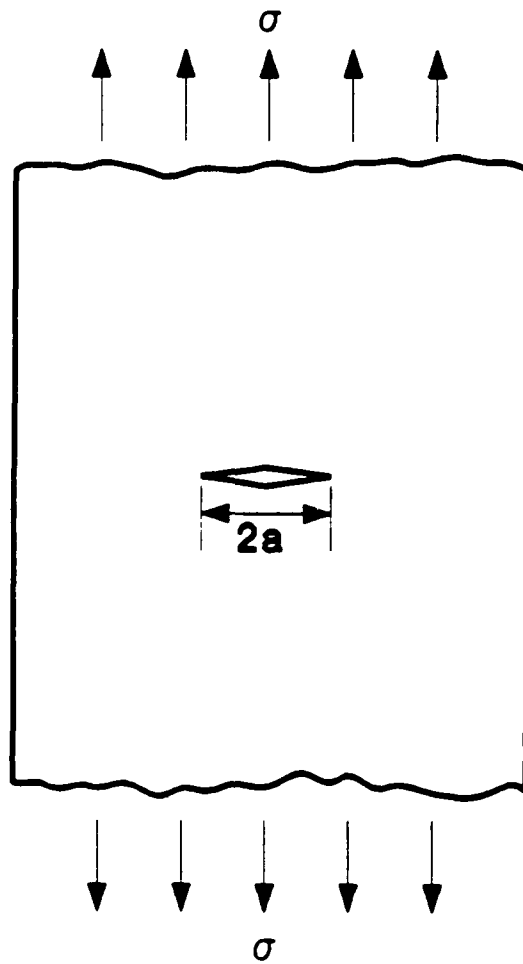
Fig. 1. Illustration of a center-cracked wide plate under a remotely applied uniform tensile stress σ. a is the half-crack length.
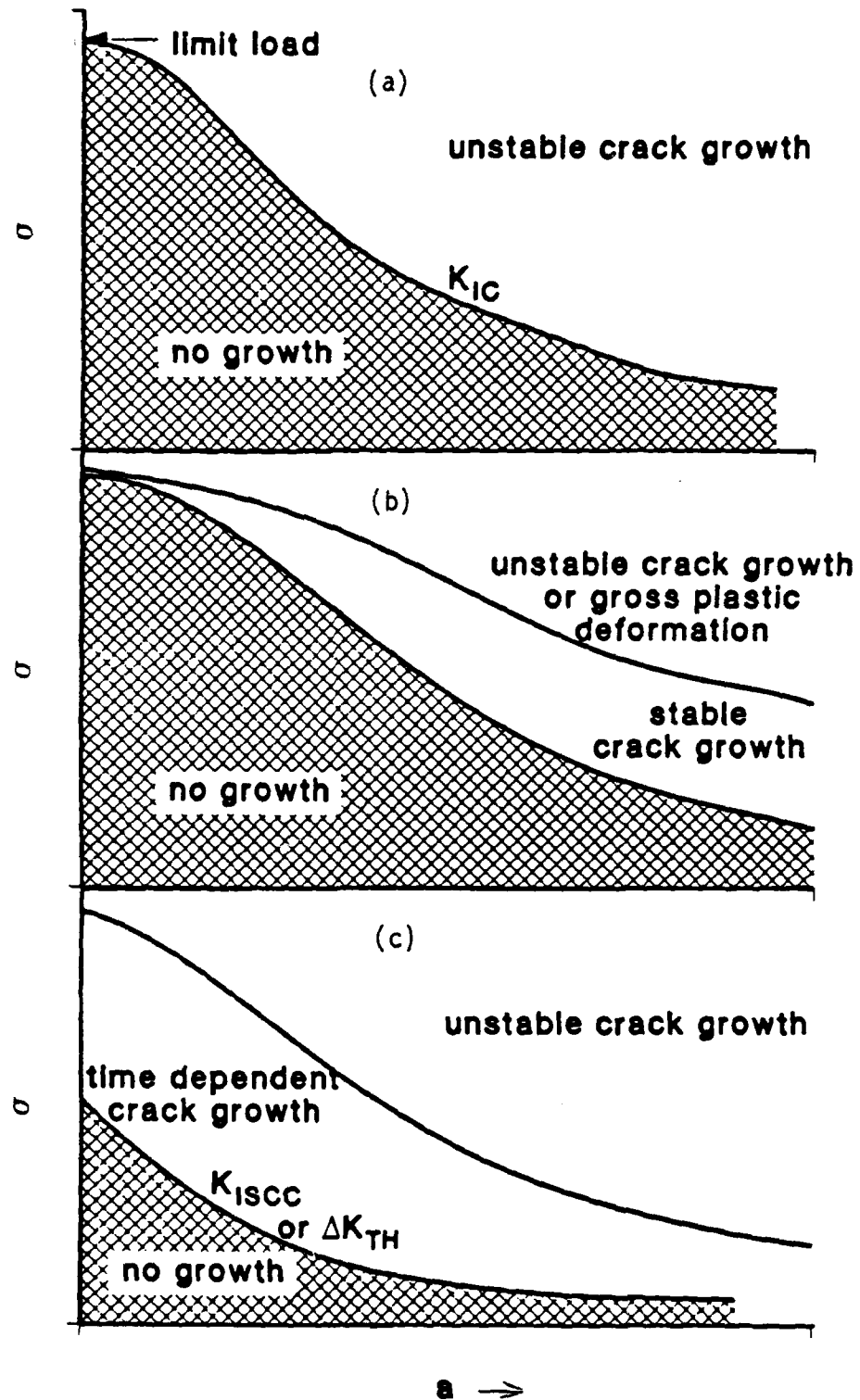
Fig. 2. Relationships between applied stress (σ) and crack length
(a) for a) linear elastic, b) elastic-plastic and c) sub-
critical crack-growth conditions.

46
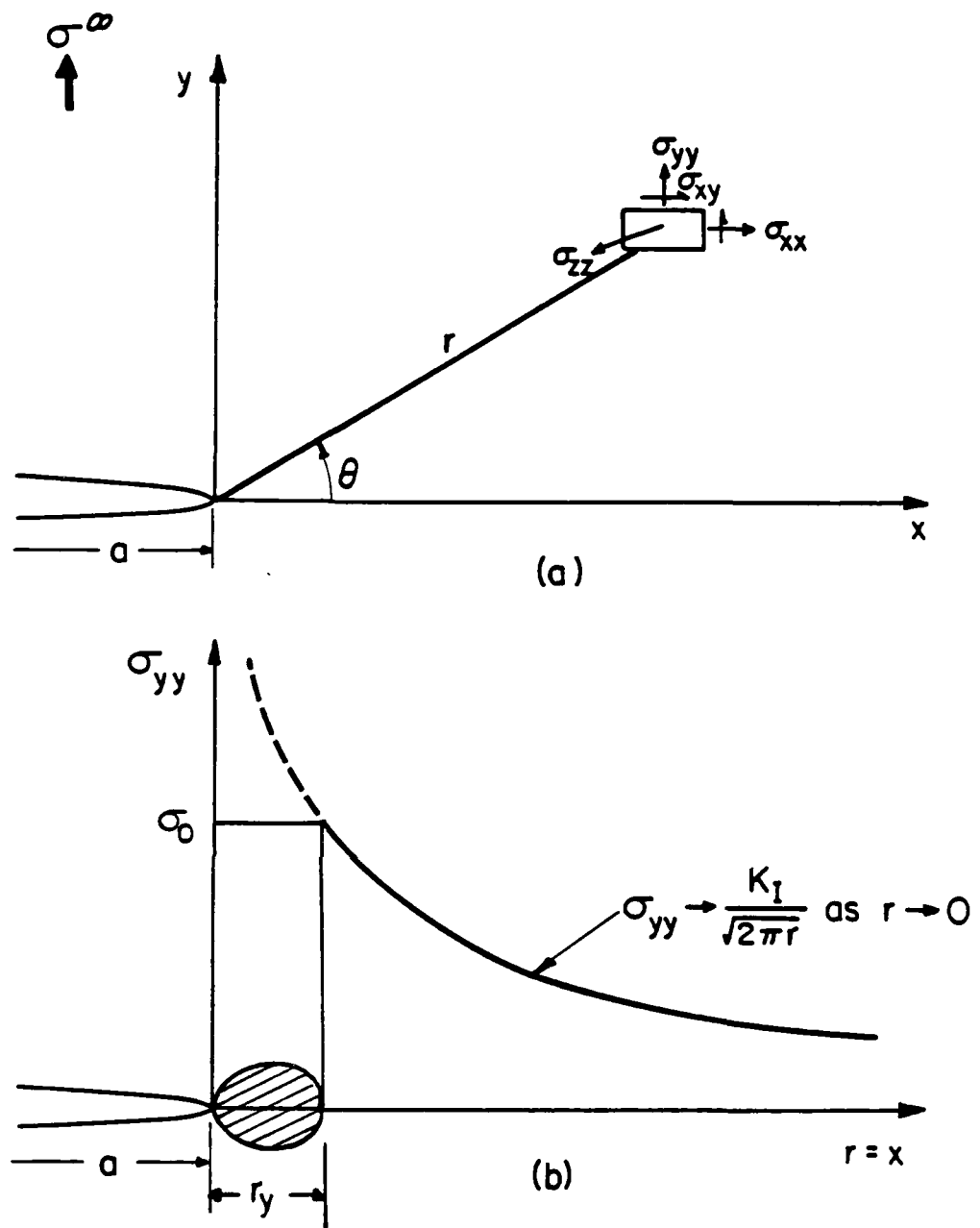
Fig. 3 Schematic representation of a half-crack, length a,
a) subjected to a Mode I remotely-applied stress σ^∞, and
b) showing the linear-elastic distribution of the local
tensile stress (σ_{yy}) directly ahead of the crack, and
approximate extent of the plastic zone size (r_y).

47
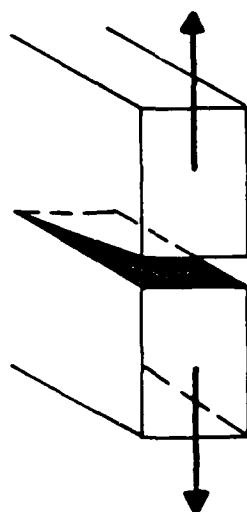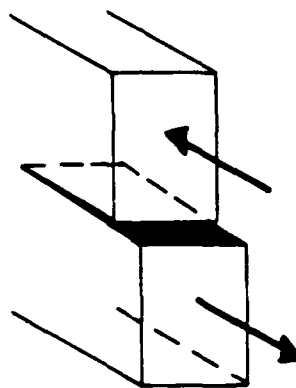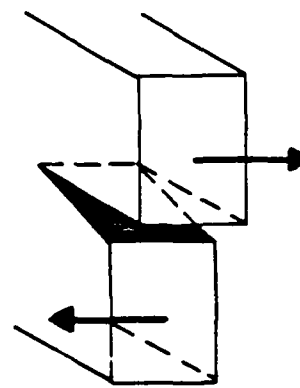
Fig. 4. Possible modes of crack separation.
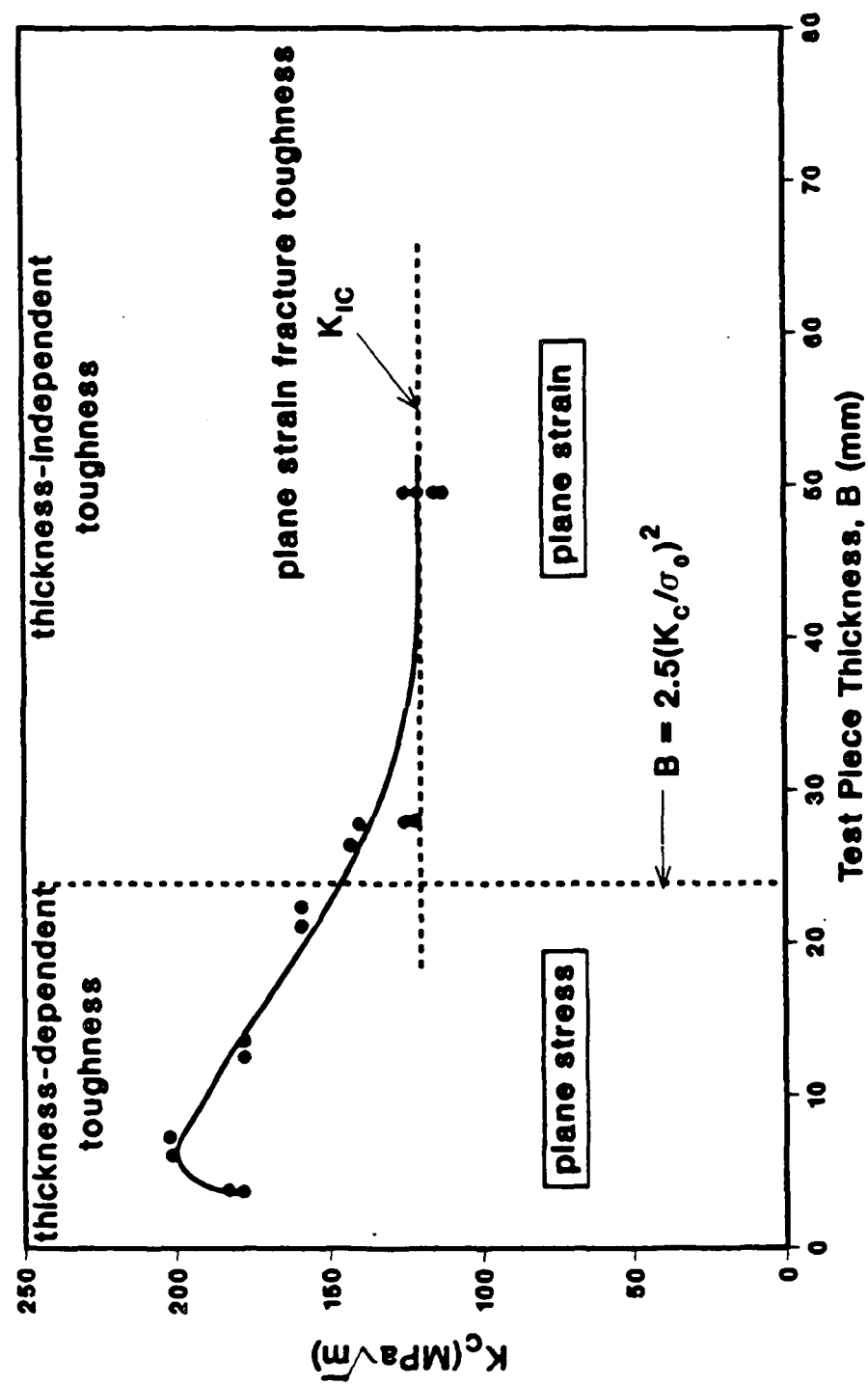
Fig. 5. Effects of test piece thickness B on the toughness (i.e., critical stress intensity at fracture K_C) of a high-strength steel ($\sigma_0 = 175$ ksi).

49
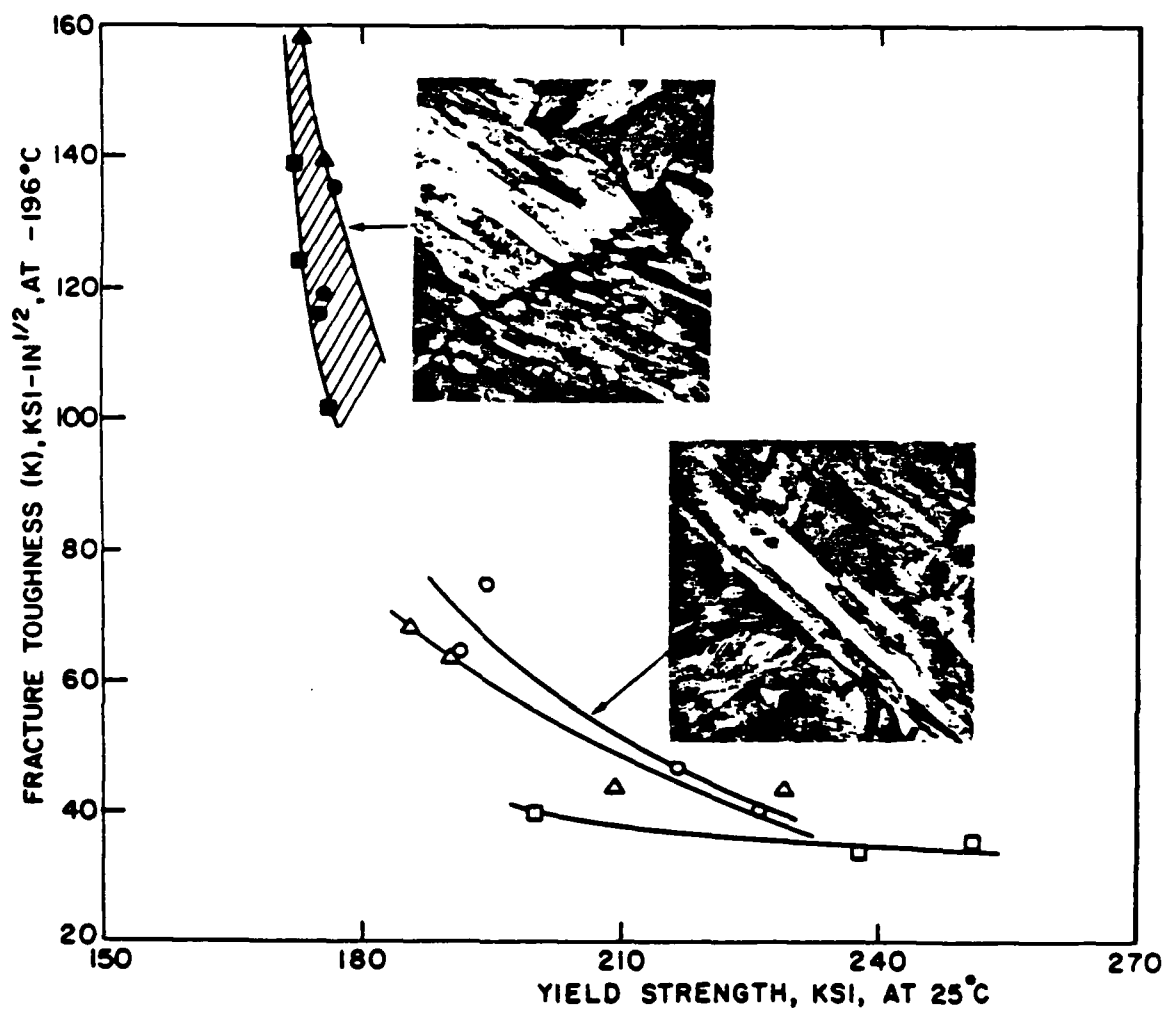
Fig. 6. Effect of yield strength on plane-strain fracture toughness K_{Ic} in medium carbon steels. In the present 0.3% C steel, the low strength is associated with a dislocated lath martensite microstructure (upper micrograph), which is much tougher than the twinned plate martensite in the higher strength microstructure (lower micrograph) (Courtesy of G. Thomas).

50
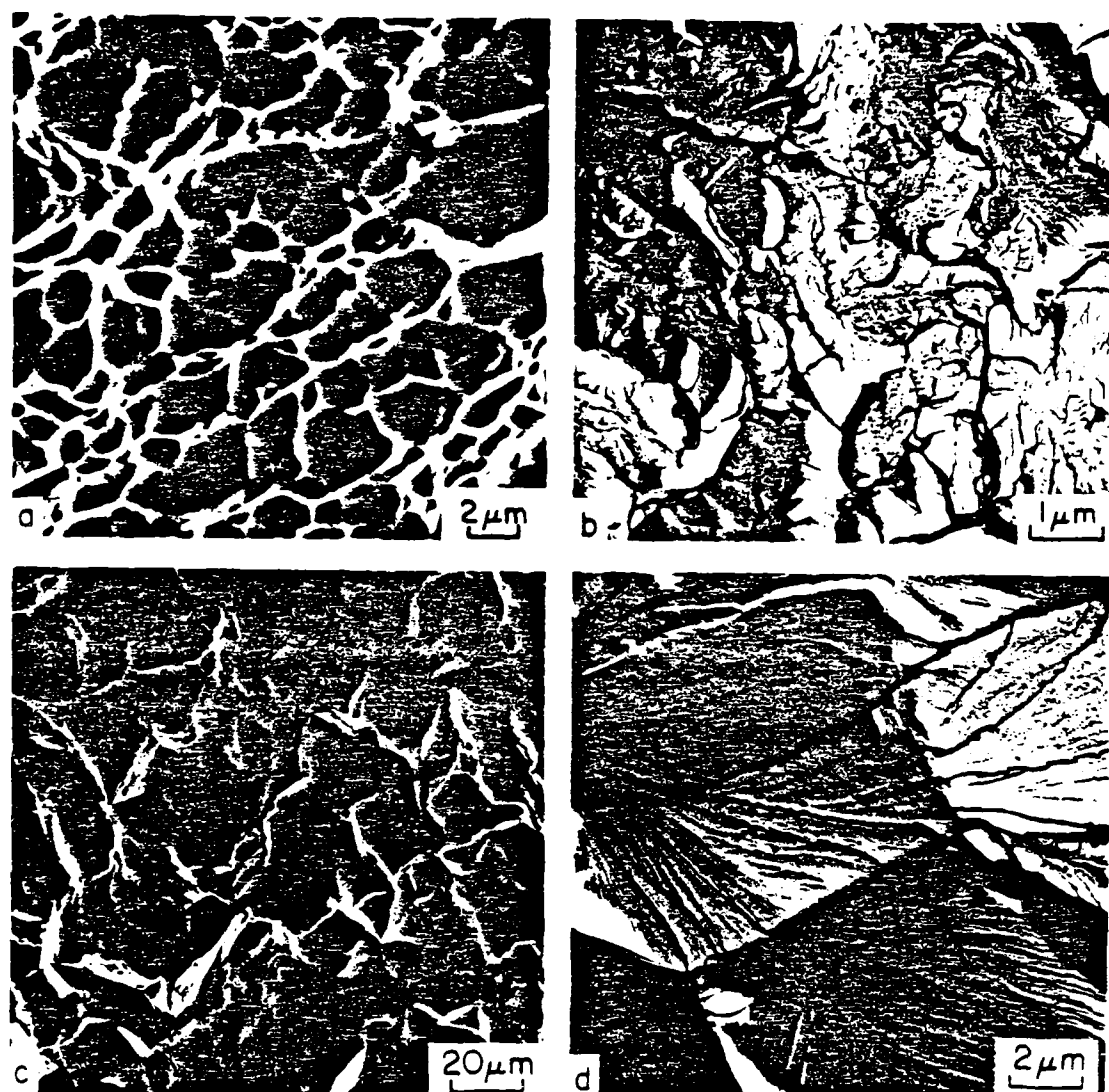
Fig. 7. Classical fracture morphologies showing a) microvoid coalescence, b) quasi-cleavage, c) intergranular cracking and d) transgranular cleavage. Fractographs a) and c) obtained using scanning electron microscopy whereas b) and d) are from transmission electron microscopy replicas (courtesy of A. W. Thompson).

51
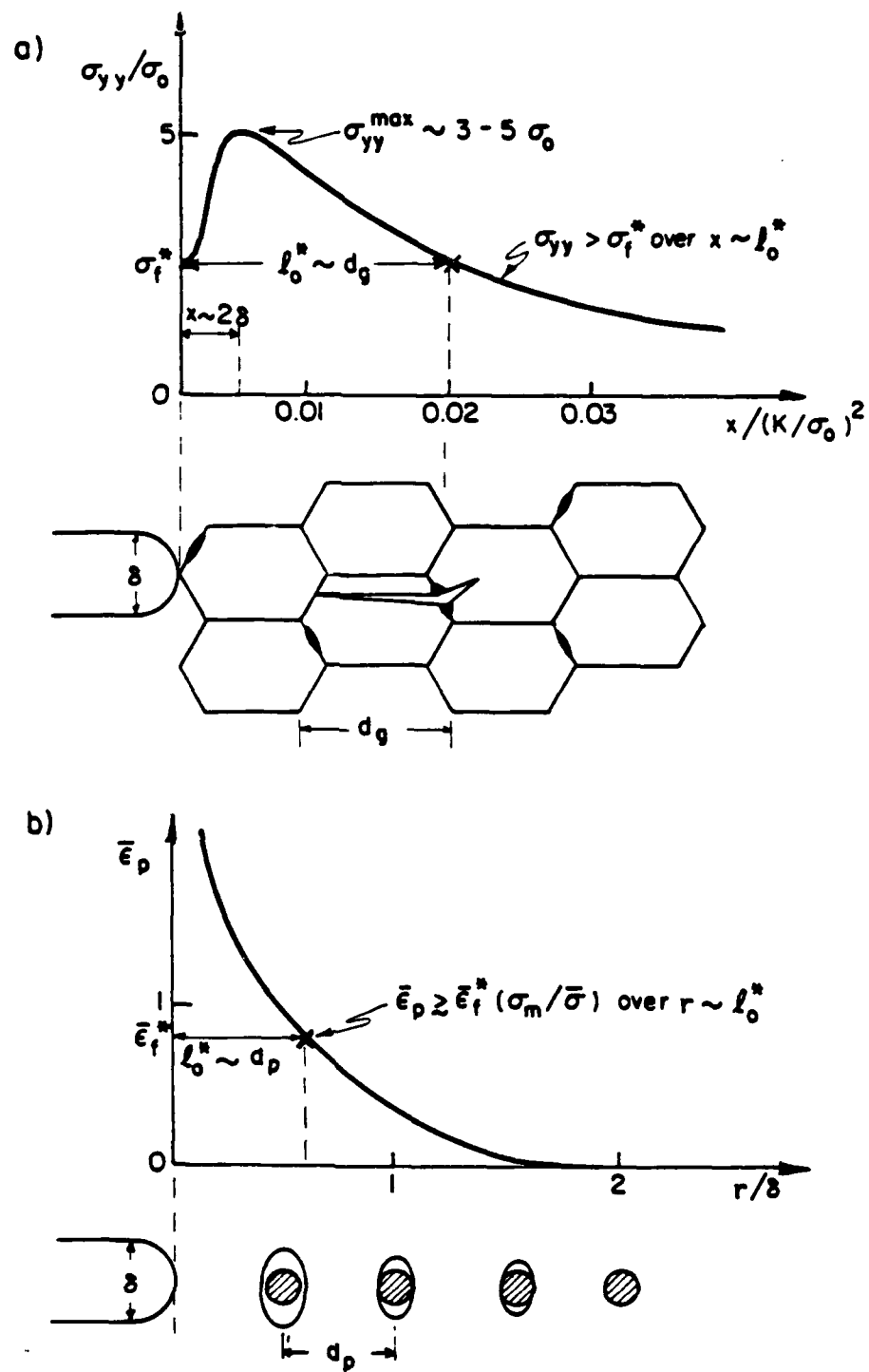
Fig. 8. Schematic idealization of microscopic fracture criteria
pertaining to a) critical stress-controlled model for
cleavage fracture and b) critical stress-modified
critical strain-controlled model for microvoid
coalescence.

52
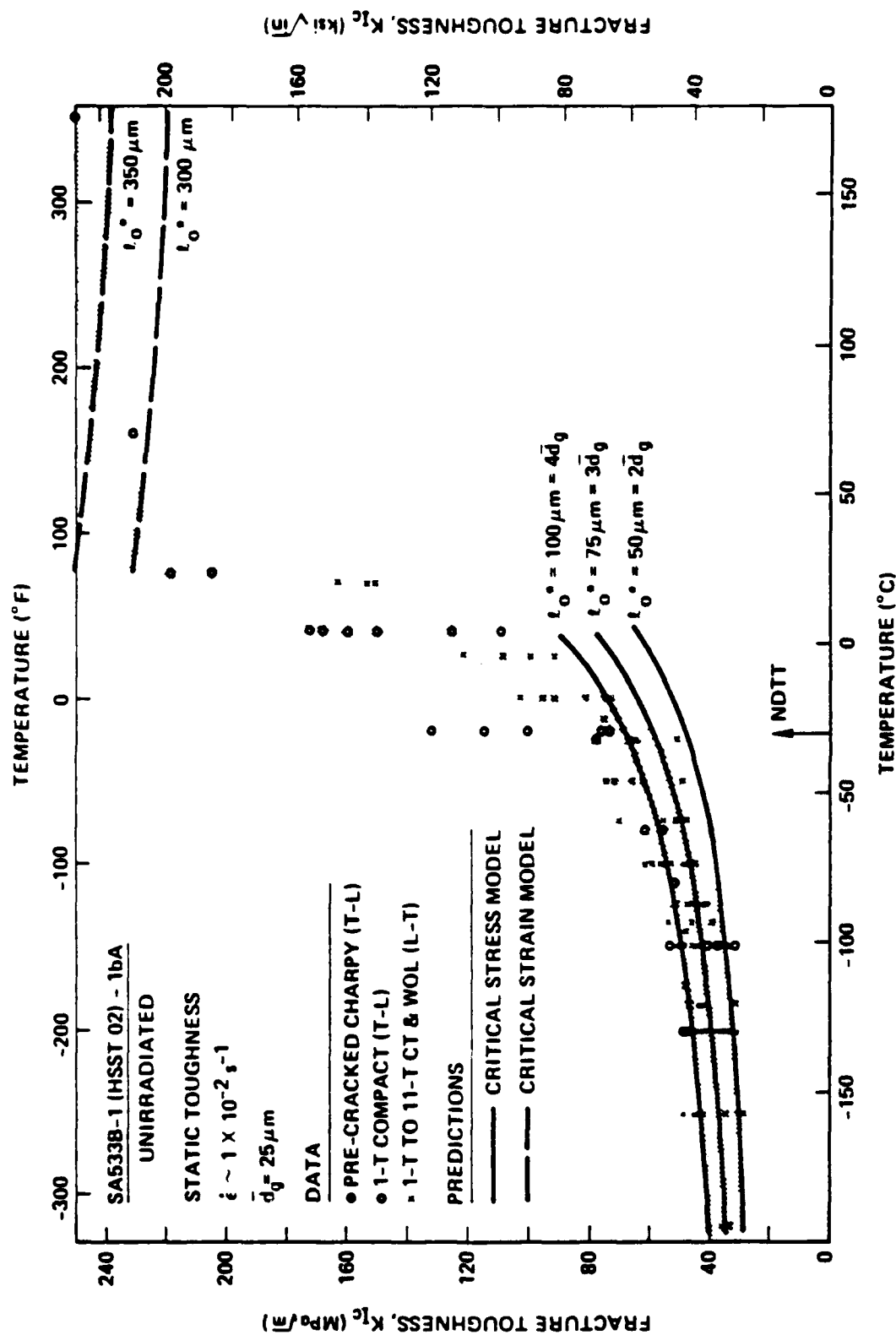
Fig. 9. Comparison of experimentally measured fracture toughness K_{Ic} data for crack initiation in SA533B-1 nuclear pressure vessel steel ($\sigma_o \sim 500$ MPa) with predicted values based on critical stress model for cleavage on the lower shelf, and on the stress-modified critical strain model for microvoid coalescence on the upper shelf.
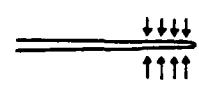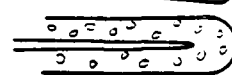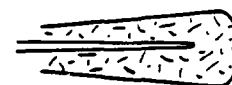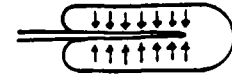
53

EXTRINSIC TOUGHENING MECHANISMS

I. CRACK DEFLECTION AND MEANDERING
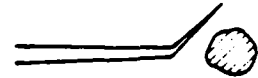
2. ZONE SHIELDING

- transformation toughening

- microcrack toughening

- crack wake plasticity

- crack field void formation

- residual stress fields

- crack tip dislocation shielding

3. CONTACT SHIELDING

- wedging:

    corrosion debris-induced crack closure

    crack surface roughness-induced closure

- bridging:

    ligament or fiber toughening

- sliding:

    sliding crack surface interference

- wedging + bridging:

    fluid pressure-induced crack closure
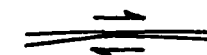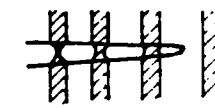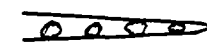
4. COMBINED ZONE AND CONTACT SHIELDING

- plasticity-induced crack closure

- phase transformation-induced closure
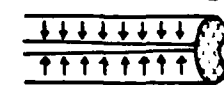
Fig. 10. Schematic illustration of classes and mechanisms of crack tip shielding.

54

Fig. 11. Schematic variation of fatigue crack propagation rate (da/dN) with stress intensity range (ΔK), showing regimes of primary growth rate mechanisms, and effects of several major variables on crack growth behavior.
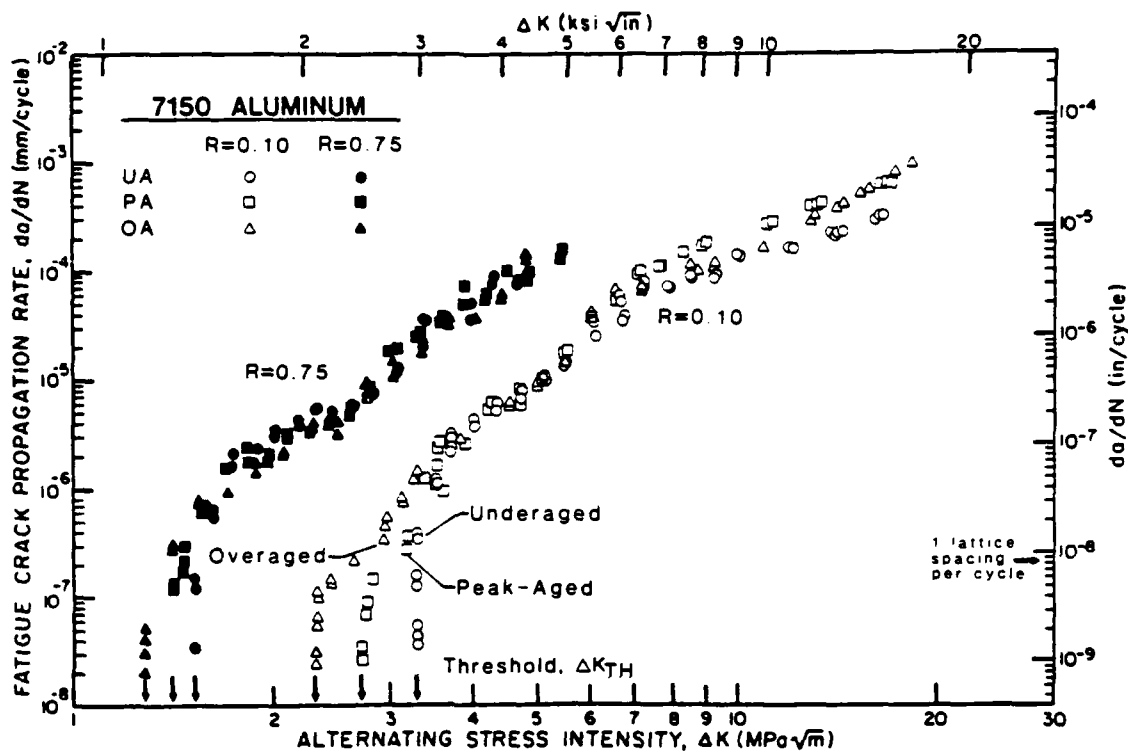
Fig. 12. Variation in fatigue crack growth rate (da/dN) as a function of stress-intensity range (ΔK) for I/M 7150 aluminum alloy Al-2%Cu-2.2%Mg-6%Zn ($\sigma_Q \sim$ 371-404 MPa) tested at R = 0.10 and 0.75 in controlled moist air. Data are shown for underaged, peak-aged (T6) and overaged (T7) microstructures.
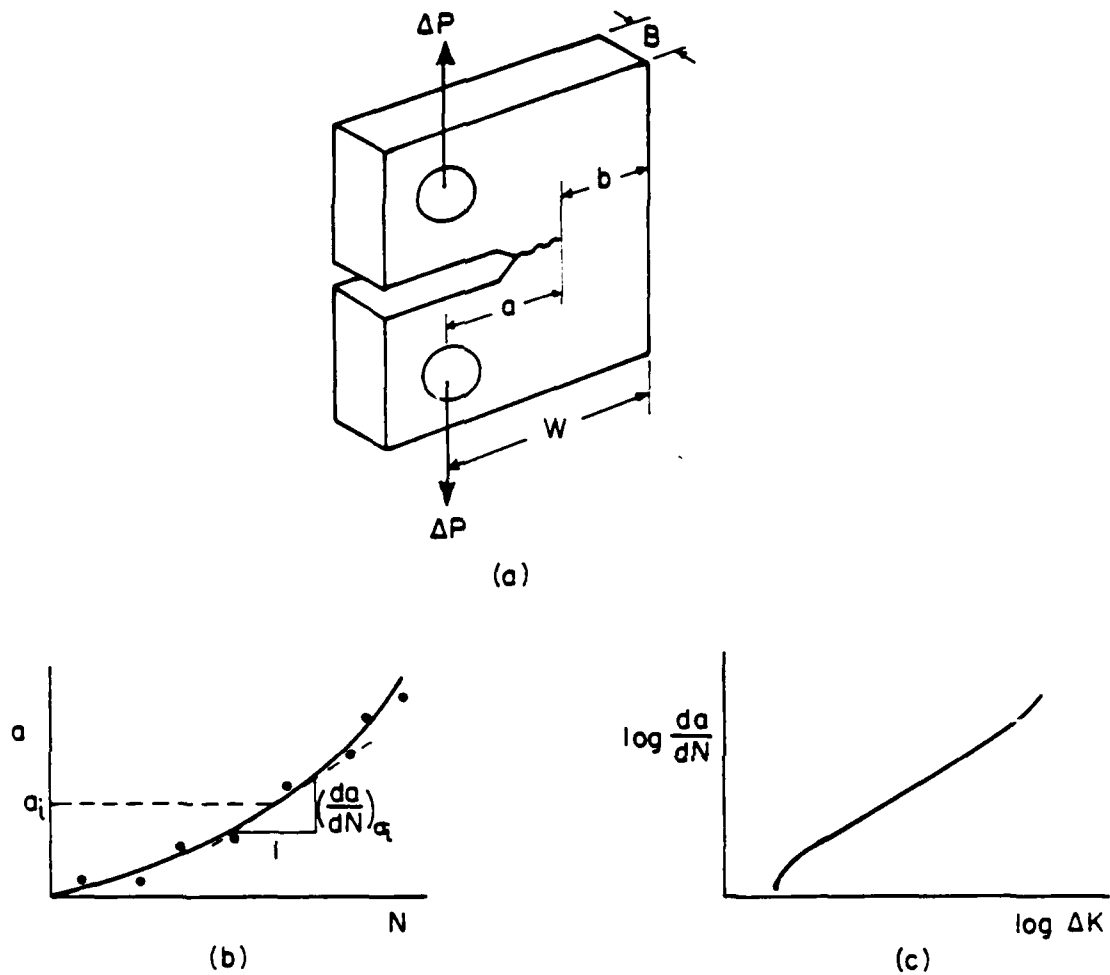
56

Fig. 13. Procedures for measuring fatigue crack propagation rates: a) compact specimen stressed under cyclic loads ΔP, b) crack length a versus number of cycles N curve differentiated to give growth rate $(da/dN)_{a_i}$ at particular crack length a_i, and c) resulting log/log plot of da/dN versus alternating stress intensity ΔK.
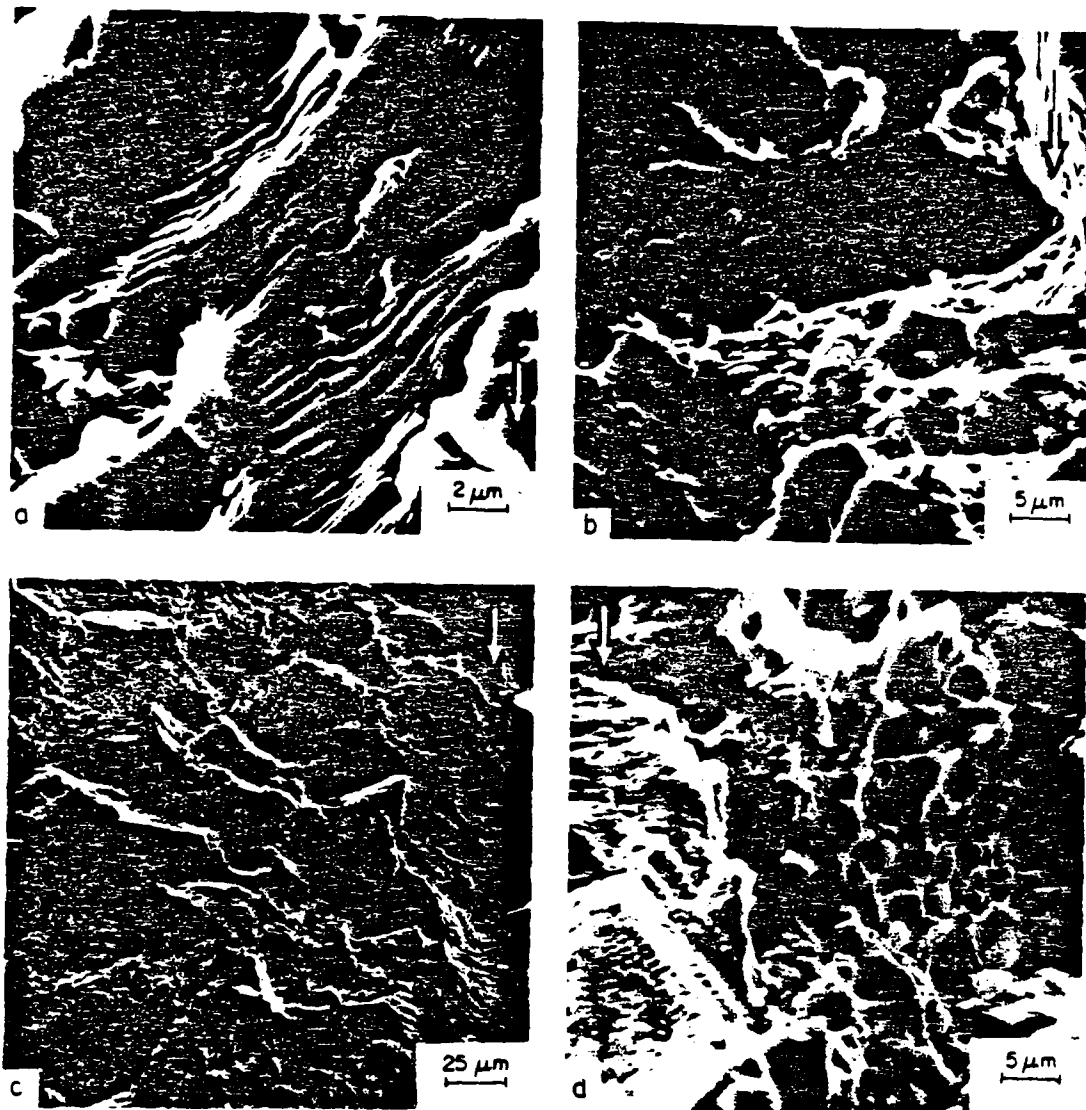
Fig. 14. Fractography of fatigue crack propagation at intermediate (regime B) and high (regime C) growth rates in steels tested in moist room air at R = 0.1, showing a) ductile striations in mild steel at ΔK = 30 MPa$\sqrt{m}$; b) additional cleavage cracking (C) during striation growth (S) in mild steel (σ_0 = 180 MPa) at ΔK = 19 MPa$\sqrt{m}$; c) additional intergranular cracking (i) in low alloy Ni-Cr steel at ΔK = 15 MPa$\sqrt{m}$; and d) additional microvoid coalescence/fibrous fracture (F) with striations (S) in AISI 316L stainless steel (σ_0 = 285 MPa) at ΔK = 30 MPa$\sqrt{m}$. Arrows indicate general direction of crack growth.

$$\Delta K = K_{max} - K_{min}$$

$$\Delta K_{eff} = K_{max} - K_{cl}$$
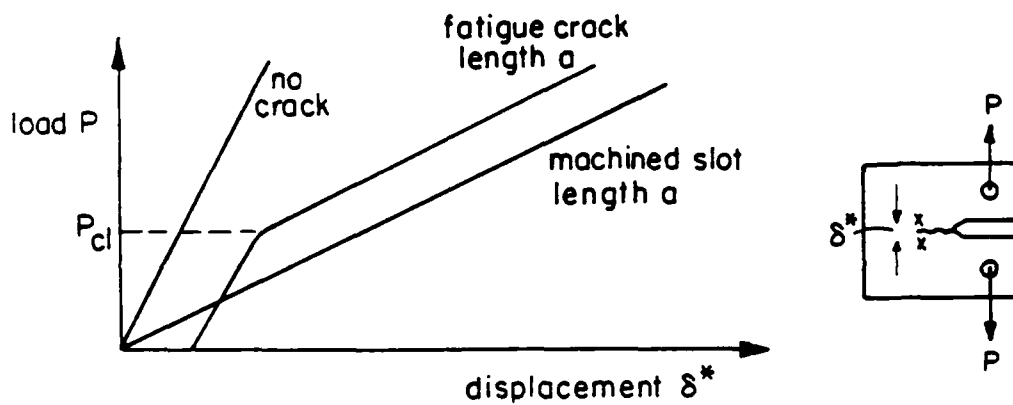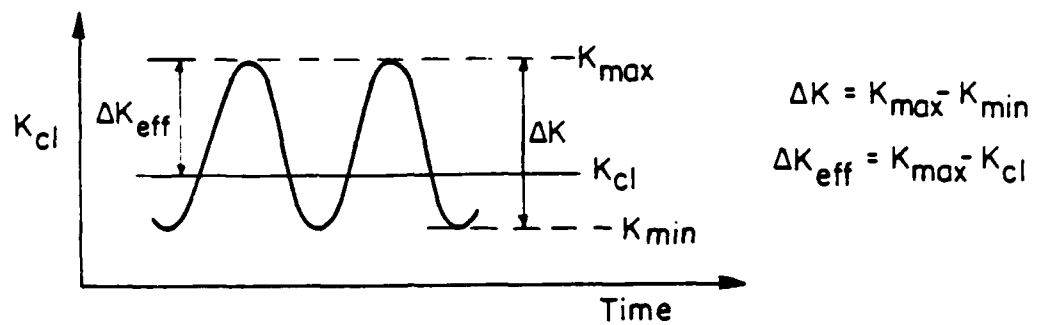
Fig. 15. Elber's procedures for experimentally demonstrating plasticity-induced crack closure, showing elastic compliance curves for uncracked test piece, test piece containing a finite width slot of length a, and test-piece containing fatigue crack of length a. Note how fatigue-cracked specimen does not appear to indicate presence of crack until above the closure load.

Fig. 16. Illustration of roughness-induced crack closure from fracture surface asperity contact during fatigue crack growth in an underaged Al-Zn-Mg (7075) aluminum alloy (courtesy of K. Schulte, H. Nowack and K. H. Trautmann, 1980).
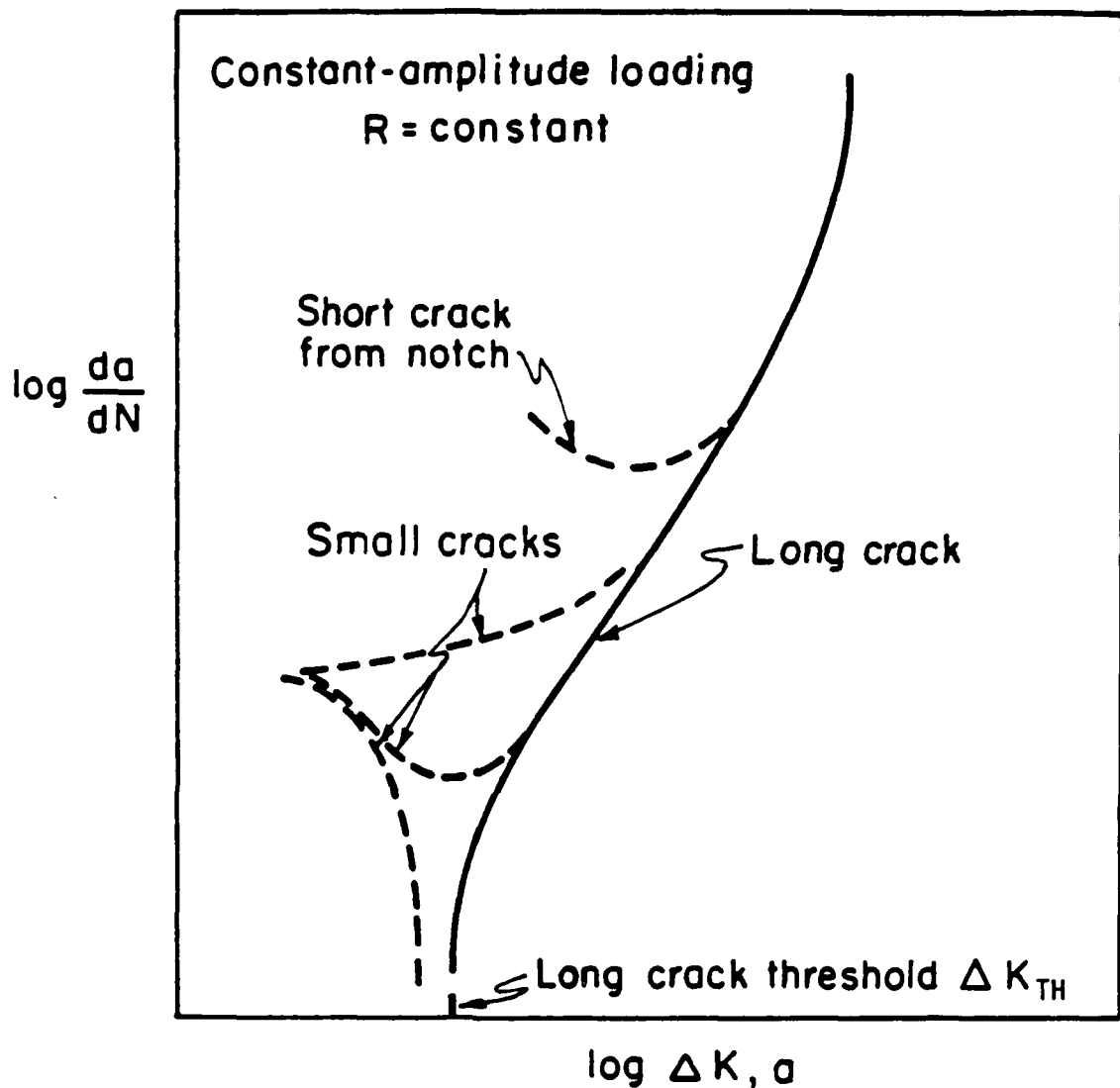
Fig. 17.   Schematic illustration of the "anomalous" fatigue crack
propagation rate (da/dN) behavior of small cracks as a
function of crack length (a) or stress intensity range
(ΔK).   Long cracks are of size where linear elastic
fracture mechanics is applicable, i.e., typically of a
length exceeding 10 mm. Small cracks of typically a size
approaching the scale of the microstructure or the extent
of local plasticity (< 1 mm).

61
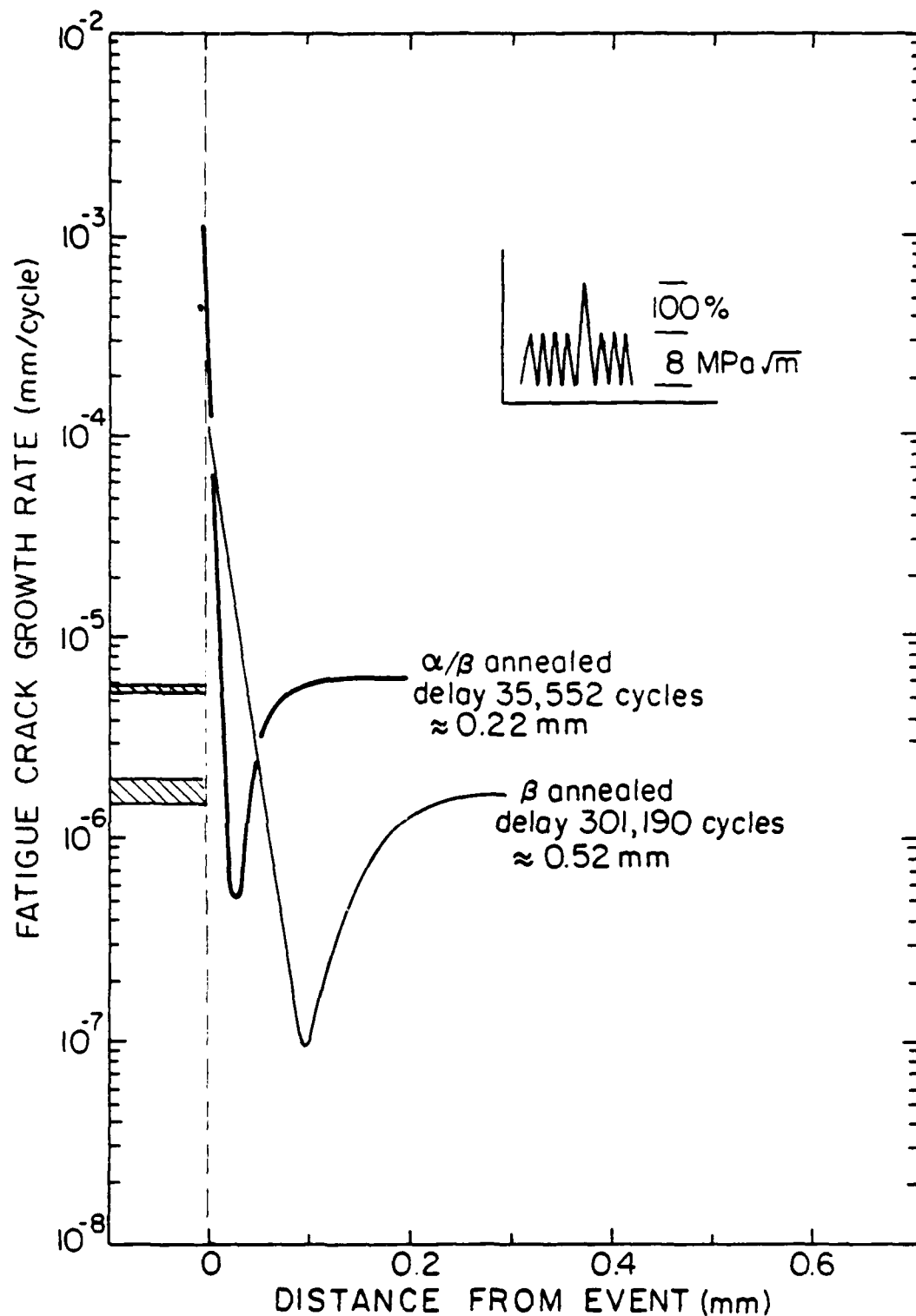
Fig. 18. Variation in fatigue crack propagation rate in α/β-annealed and β-annealed microstructures of an IMI 550 titanium alloy Ti-4Al-4Mo-2Zn (σ_0 = 1024 and 888 MPa, respectively), following single 100% single tensile overload cycles applied to a baseline ΔK of 8 MPa√m. Note how the growth rate initially accelerates before undergoing a significant delayed retardation.

62

K (ksi √in.)

STRESS CORROSION CRACK GROWTH RATE , da/dt, (mm/sec)

da/dt (inches/sec)

K_{Ic}

K_{Iscc}

AISI 4340 and 300-M
Distilled Water at 23°C
Constant Yield Strength = 1497 MPa

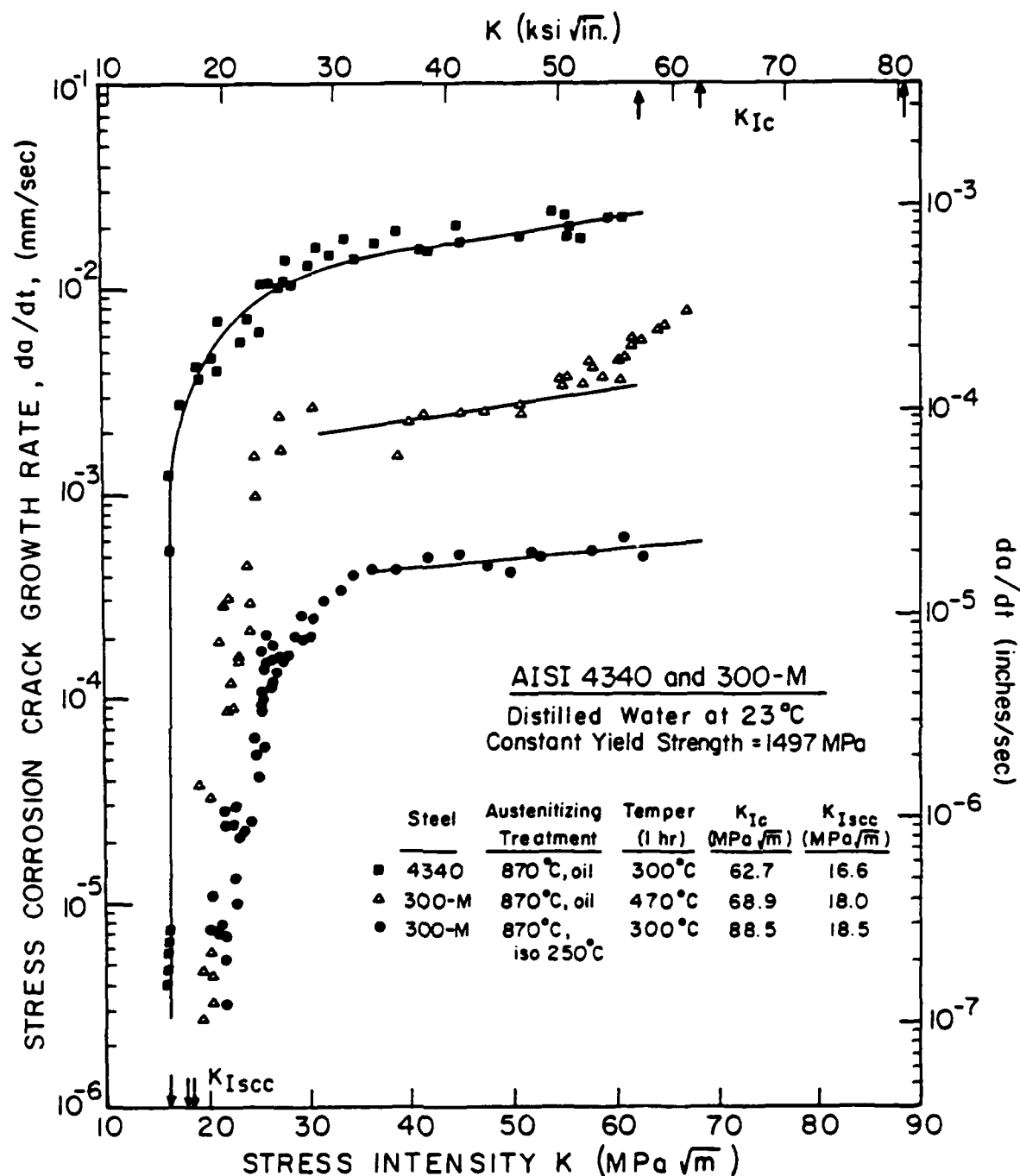| Steel	Austenitizing Treatment	Temper (1 hr)	K_{Ic} (MPa√m)	K_{Iscc} (MPa√m)
4340	870°C, oil	300°C	62.7	16.6
300-M	870°C, oil	470°C	68.9	18.0
300-M	870°C, iso 250°C	300°C	88.5	18.5

STRESS INTENSITY K (MPa √m)

Fig. 19. Variation of stress corrosion crack growth rate (da/dt)
with instantaneous stress intensity (K) for 4340 and 300-
M steels (Fe-0.4C-1.7Ni-0.7Cr), heat-treated by quench
and tempering and by isothermal transformation to give
identical yield strength of σ_0 = 1497 MPa. Tests were
performed in distilled water at ambient temperature.

63

TECHNICAL REPORT INTERNAL DISTRIBUTION LIST

	NO. OF COPIES
CHIEF, DEVELOPMENT ENGINEERING BRANCH	
ATTN: SMCAR-CCB-D	1
-DA	1
-DC	1
-DM	1
-DP	1
-DR	1
-DS (SYSTEMS)	1
CHIEF, ENGINEERING SUPPORT BRANCH	
ATTN: SMCAR-CCB-S	1
-SE	1
CHIEF, RESEARCH BRANCH	
ATTN: SMCAR-CCB-R	2
-R (ELLEN FOGARTY)	1
-RA	1
-RM	1
-RP	1
-RT	1
TECHNICAL LIBRARY	5
ATTN: SMCAR-CCB-TL	
TECHNICAL PUBLICATIONS & EDITING UNIT	2
ATTN: SMCAR-CCB-TL	
DIRECTOR, OPERATIONS DIRECTORATE	1
ATTN: SMCWV-OD	
DIRECTOR, PROCUREMENT DIRECTORATE	1
ATTN: SMCWV-PP	
DIRECTOR, PRODUCT ASSURANCE DIRECTORATE	1
ATTN: SMCWV-QA	

NOTE: PLEASE NOTIFY DIRECTOR, BENET LABORATORIES, ATTN: SMCAR-CCB-TL, OF ANY ADDRESS CHANGES.

TECHNICAL REPORT EXTERNAL DISTRIBUTION LIST

	NO. OF COPIES		NO. OF COPIES
ASST SEC OF THE ARMY RESEARCH AND DEVELOPMENT ATTN: DEPT FOR SCI AND TECH THE PENTAGON WASHINGTON, D.C. 20310-0103	1	COMMANDER ROCK ISLAND ARSENAL ATTN: SMCRI-ENM ROCK ISLAND, IL 61299-5000	1
ADMINISTRATOR DEFENSE TECHNICAL INFO CENTER ATTN: DTIC-FDAC CAMERON STATION ALEXANDRIA, VA 22304-6145	12	DIRECTOR US ARMY INDUSTRIAL BASE ENGR ACTV ATTN: AMXIB-P ROCK ISLAND, IL 61299-7260	1

COMMANDER
US ARMY ARDEC
ATTN: SMCAR-AEE
   SMCAR-AES, BLDG. 321
   SMCAR-AET-O, BLDG. 351N
   SMCAR-CC
   SMCAR-CCP-A
   SMCAR-FSA
   SMCAR-FSM-E
   SMCAR-FSS-D, BLDG. 94
   SMCAR-MSI (STINFO)
PICATINNY ARSENAL, NJ 07806-5000
	1
	1
	1
	1
	1
	1
	1
	1
	2
		COMMANDER
		US ARMY TANK-AUTMV R&D COMMAND
		ATTN: AMSTA-DDL (TECH LIB)
		WARREN, MI 48397-5000
		
		COMMANDER
		US MILITARY ACADEMY
		ATTN: DEPARTMENT OF MECHANICS
		WEST POINT, NY 10996-1792
		
		US ARMY MISSILE COMMAND
		REDSTONE SCIENTIFIC INFO CTR
		ATTN: DOCUMENTS SECT, BLDG. 4484
		REDSTONE ARSENAL, AL 35898-5241
			1
			
			1
			
			2

DIRECTOR US ARMY BALLISTIC RESEARCH LABORATORY ATTN: SLCBR-DD-T, BLDG. 305 ABERDEEN PROVING GROUND, MD 21005-5066	1	COMMANDER US ARMY FGN SCIENCE AND TECH CTR ATTN: DRXST-SD 220 7TH STREET, N.E. CHARLOTTESVILLE, VA 22901	1
DIRECTOR US ARMY MATERIEL SYSTEMS ANALYSIS ACTV ATTN: AMXSY-MP ABERDEEN PROVING GROUND, MD 21005-5071	1	COMMANDER US ARMY LABCOM MATERIALS TECHNOLOGY LAB ATTN: SLCMT-IML (TECH LIB) WATERTOWN, MA 02172-0001	2
COMMANDER HQ, AMCCOM ATTN: AMSMC-IMP-L ROCK ISLAND, IL 61299-6000	1		

NOTE: PLEASE NOTIFY COMMANDER, ARMAMENT RESEARCH, DEVELOPMENT, AND ENGINEERING CENTER, US ARMY AMCCOM, ATTN: BENET LABORATORIES, SMCAR-CCB-TL, WATERVLIET, NY 12189-4050, OF ANY ADDRESS CHANGES.

	NO. OF COPIES		NO. OF COPIES
COMMANDER US ARMY LABCOM, ISA ATTN: SLCIS-IM-TL 2800 POWDER MILL ROAD ADELPHI, MD 20783-1145	1	COMMANDER AIR FORCE ARMAMENT LABORATORY ATTN: AFATL/MN EGLIN AFB, FL 32542-5434	1
COMMANDER US ARMY RESEARCH OFFICE ATTN: CHIEF, IPO P.O. BOX 12211 RESEARCH TRIANGLE PARK, NC 27709-2211	1	COMMANDER AIR FORCE ARMAMENT LABORATORY ATTN: AFATL/MNF EGLIN AFB, FL 32542-5434	1
DIRECTOR US NAVAL RESEARCH LAB ATTN: MATERIALS SCI & TECH DIVISION CODE 26-27 (DOC LIB) WASHINGTON, D.C. 20375	1 1	METALS AND CERAMICS INFO CTR BATTELLE COLUMBUS DIVISION 505 KING AVENUE COLUMBUS, OH 43201-2693	1

NOTE: PLEASE NOTIFY COMMANDER, ARMAMENT RESEARCH, DEVELOPMENT, AND ENGINEERING CENTER, US ARMY AMCCOM, ATTN: BENET LABORATORIES, SMCAR-CCB-TL, WATERVLIET, NY 12189-4050, OF ANY ADDRESS CHANGES.